Politecnico di Torino

POLITECNICO DI TORINO

Master's Degree in Nanotechnologies for ICTs

Master's Degree Thesis

Analysis of piezoionic phenomenon in ionic liquid based polymer for wearable application

Supervisor
prof. STASSI Stefano

Candidate
VENZA Francesco Paolo

July 2024

Abstract

Pressure sensing based on polymeric materials offers a wide array of advantages, from high deformability and conformability to the human skin to the possibility of exploiting ionic conduction for human-machine interfaces. Among the electromechanical transduction mechanisms object of study, a novel phenomenon named the piezoionic effect has recently gained recognition for its ability to produce bio-inspired signals in both charged and uncharged polymeric matrices.
In this thesis, samples composed of a neutral cellulose matrix and fabricated through DLP 3D printing are first characterized to assess the influence of geometry on their electrical response. Then, an ionic liquid formulation is polymerized to obtain samples with a charged network which are characterized for their mechanical and electrical response through tensile and compressive stimuli. Finally, the sensors are used as piezoionic physiological signals transducers. This paves the way for the rapid prototyping of flexible sensors with tunable responses and self-powering capabilities for biomedical and energy-harvesting applications.

Table of Contents

List of Tables

List of Figures

Chapter 1

Introduction

The human body is capable of translating external stimuli to electrical pulses as it interacts with the world. The skin, being the body's largest organ, has a fundamental role in this regard. The work of many around the world is focused on trying to replicate the skin's mechanical-to-electric transduction abilities. The field of piezoionics has recently attracted increasing attention since its implementation offers a viable alternative to devices based on resistance/capacitance variation or contact electrification.
As it stands, the piezoionic effect concerns a displacement of ions inside a solvent infused polymeric matrix subjected to pressure, a displacement which is able to generate an electrical signal.
This novel paradigm can be employed for the fabrication of easy-to-integrate and self-powered devices, ready for use in the IoT (Internet of Things). The biomedical field can also benefit greatly from exploring this phenomenon, as the ionically conductive hydrogel materials used are soft and compliant and the signals generated are bio-inspired.

The thesis work starts in Chapter 1 with a brief introduction on the state of the art of flexible sensors, highlighting the peculiarity of exploiting this new transduction mechanism.
In Chapter 2, the ionic liquid based formulation and cellulose samples utilized for the study are presented, along with the characterization methods used. Chapter 3 focuses on the results and discussion of the mechanical and electromechanical tests performed, along with applications of the sensor developed. Finally, in Chapter 4, conclusions are laid out and possible future studies proposed.

1.1 Tactile sense

The sense of touch in mammals occurs through mechanoreceptors, which are sensory neurons able to transduce an external stimulus (in this case a mechanical deformation) into an action potential by means of a mechanically-gated ion channel. The cell membrane potential reacts to an high enough stimulus by changing its resting value of about -70 mV and becoming positive. As the deformation is released, the potential returns to its resting state (Figure 1.1).

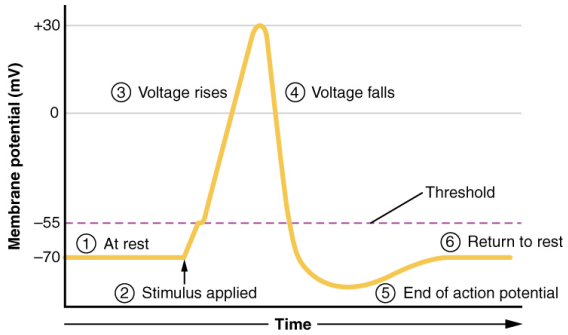

Figure 1.1: Membrane voltage alteration during tactile sensing [1]

The gated release of Na_+ ions produces a change in the electrical charge of the membrane, releasing neurotransmitters which then act on another cell to produce an action potential.
The magnitude of the receptor potential influences the frequency at which pulses are generated and is mainly influenced by which particular sensory cell is stimulated.

Mechanoreceptors, as thoroughly explained in [2], in can be distinguished by different characteristics:

- Adaptation rate: measures the ability of the receptor to follow the stimulus applied in time (Figure 1.2). The distinction is between fast-adapting (i.e. response to rapid taps) and slow-adapting (i.e. stretching of the skin due to joint motion)
- Size of receptive field: indicates the size of the area around the receptor through which the stimulus propagates and can be detected by a single neuron
- Intensity of stimulus detected: the distinction is between HTMR (High Threshold Mechanoreceptors, also called nociceptors) whose role is to respond to damaging stimuli by sending signals to the brain and the spinal cord and LTMR (Low Threshold Mechanoreceptors).

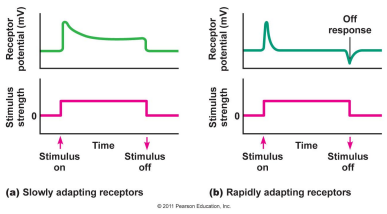

Figure 1.2: Adaptation rate of cutaneous mechanoreceptors

Among the low threshold mechanoreceptors are Meissner Corpuscles and Merkel discs located closer to the skin surface and reactive to stimuli confined to a small area. Deep down are Pacinian corpuscles (in the dermis) and Ruffini endings (in the subcutaneous tissue), whose sensory reach is extended with respect to the former ones.

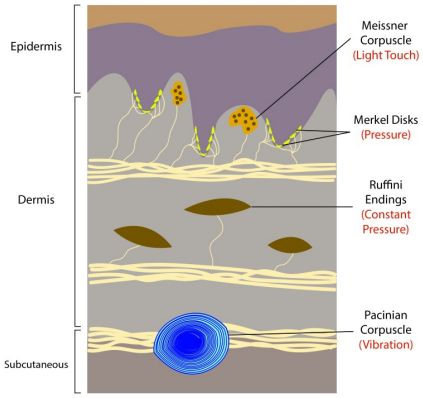

Figure 1.3: Location of cutaneous mechanoreceptors in the skin [3]

In rapid adapting receptors, the response to mechanic solicitation (seen as a train of pulses due to the action potential discharge) is confined to the time frame of force application and force removal. In slow adapting receptors, the discharge happens even when the force stimulus is held constant.
In small receptive field receptors, the depolarization following the initial contact with the skin causes a rapid increase in the rate of discharge, differently from their large receptive-field counterparts.

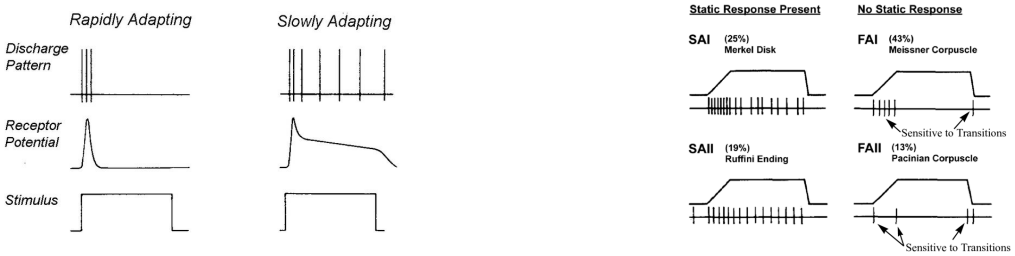

Figure 1.4: (left) adaption rate of mechanoreceptors [4] and (right) receptive field [5].

Recent studies focus on creating syntethic mechanoreceptors which are responsive to various stimuli. Recently, Lin et al. [6] have fabricated a tactile sensors incorporanting a BSM (biomimetic slow-adapting mechanoreceptor) based on a bottom layer of polydimethylsiloxane (PDMS), with rGO (reduced Graphene Oxide) and silver nanowires (AgNWs) electrode, a middle layer of a porous elastomer and a top PDMS layer with an interdigitated electrode. Bimodal sensing was achieved thanks to the PDMS layers responding to lateral strain (simulating SA-II receptors) while being insensitive to contact pressure, which was instead detected by the porous middle layer.

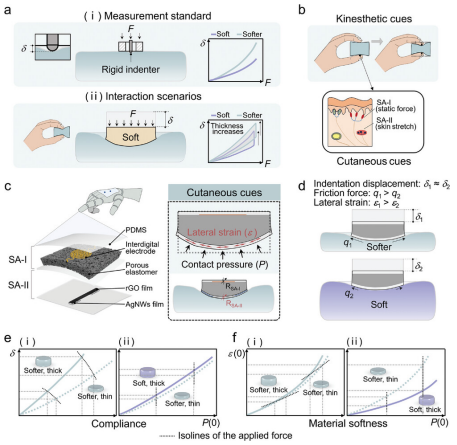

Figure 1.5: Biomimetic slow adapting mechanoreceptor [6]

As it stands, soft materials of the like of elastomers or hydrogels seem to be the most convenient option for recreating the sense of touch.

1.2 Flexible wearable sensors

The advancement in human-machine interfaces and soft robotics [7], fueled by the recent progresses in Machine Learning (ML) and AI, and the ever-present need for biomedical devices able to monitor body parameters of patients (such as hearth pulse rate, pulse wave velocity, tremors, etc.) require mechanical transductors with a high degree of pliability and conformability.
Flexible pressure sensors based on polymeric materials are one of the many responses to these challenges. Pliability is only one of the desirable characteristics in one such device, others [8] [9] are:

- low hysteresis: hysteresis is generally defined as a system change which depends on the history of the applied perturbation and in the realm of pressure sensors this translates into a variation in deformation magnitude depending on the history of the applied load. Hysteresis in flexible pressure sensors is mainly related to the viscoelastic properties of the material: contrary to elastic materials, part of the energy in the loading-unloading cycle is dissipated as heat. Hysteresis may also be due to fillers, as reported in [10], where different concentration of glass microspheres in an elastomer introduced a residual strain and variable degree of hysteresis in samples subjected to cyclic loading.

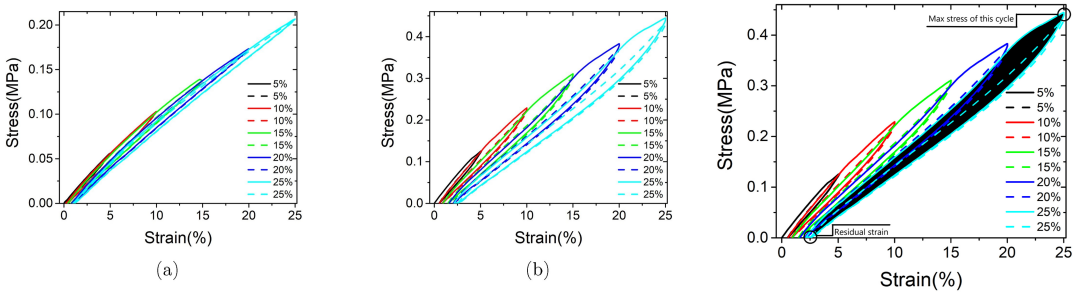

Figure 1.6: (left) filler-mediated hysteresis change: neat elastomer (a) and with glass microsphere (b) and (right) residual strain and area of hysteresis loop [10].

The degree of hysteresis is given by:

$$DH = \frac{A_{unloading} - A_{loading}}{A_{loading}} \times 100\% \tag{1.1}$$

with $A_{loading}$ and $A_{unloading}$ the area under the loading and unloading curve in the stress-strain graph, respectively;

- fast response/recovery time: the inherent hysteresis present in viscoeleastic materials brings about a delay in the electrical signal, which translates in

usually two time constants characterizing in the electrical response of the sensor to the load applied: response time and recovery time. The first denotes the rising edge of the signal generated and quantifies the time needed to reach 90% of its maximum value and can be influenced by the device setup and the conditioning circuit.The second is related to the falling edge (time to reach 10% of final value after step unloading) and is mainly influenced by the flexible material's properties;

- high sensitivity and resolution: sensitivity in a sensor is defined as $S = \frac{\Delta output}{\Delta input}$, meaning relative variation of the measurand output with respect to the input (either a uniaxial strain deformation or normal pressure). Sensititivity may be increased by embedding chemical additives or nanofillers in the polymeric matrix. Resolution, on the other hand, is the minimum incremental change in the input which produces and appreciable output;

- broad working range, as in ability to detect a wide array of mechanical solicitations. The lower boundary of this range is the limit of detection (LOD) and denotes the minimum input that can be observed with a sufficient degree of reliability;

- directional sensing, as in ability to discern where the external stimulus has interacted with the material. This property in particular is also dependent on the location of the electrodes, since the pressure signal must travel through the material before being detected and recorded;

- stable performances, which concerns the ability of a device to maintain its structural and sensing properties after being subjected to extensive usage and/or adverse conditions (temperature, humidity, etc.);

- a sufficient degree of transparency, which is usually preferred if the device has to be integrated on a larger biomedical platform. Biocompatibility and air/sweat permeability are also highly sought characteristics in this regard;

- ability to couple the mechanical force stimulation with an electrical signal, which usually translates into a detectable variation of resistance, capacitance, voltage or current;

The transduction mechanism allows one to arrange flexible pressure sensors into categories, whose main differences and notable examples (taken from the literature) are briefly discussed below.

1.2.1 Piezoresistance sensors

Resistive sensors detect a change in the electrical resistance of a device, which is defined as:

$$R = \rho \frac{l}{A} \tag{1.2}$$

where ρ is the intrisic resistivity of the material, l the length and A the section of the portion of conductive material under consideration).
The sensitivity in these sensors is called Gauge Factor (GF):

$$GF = \frac{\frac{\Delta R}{R_0}}{\Delta X} \tag{1.3}$$

where ΔR is the resistance variation, R_0 the initial resistance of the sample and ΔX is usually the engineering strain ϵ or a pressure variation to which the sensor is subjected.
Common strategies to increase the sensitivity of piezoresistive pressure sensors include the suitable choice and concentration of conductive filler, usually metal (Ag, carbon) nanoparticles and the microscale engineering of the interface between electrode and conductive material. For example, Huang et al. [11] demonstrated an hybrid aerogel/hydrogel made of PPy nanotubes (prepared through sacrificial templating on Cu nanowires) embedded in a PAAm hydrogel.The aereogel by itself exhibited exceptional compressibility and recovery and good sensitivity. The sensor's working range was extended through the PAAm hydrogel network, allowing to sense and (more importantly) whitstand even a car passing over it (as shown in Figure 1.7).
The piezoresistance transduction mechanism has the inherent advantages of leading to devices with a low power consumption, which tends to increase if an active conditioning circuit or readout tool are needed. Moreover, temperature drift is problematic and is due to the fact that the polymeric chains tend to be more mobile at increasing temperature, which in turns reduces the Young modulus' of the material and decreases the sensitivity to compressive/tensile strain [12].

1.2.2 Piezocapacitive sensors

A capacitor is a device composed of a dielectric layer sandwiched between two electrodes (armature plates). An electric field applied to a capacitor polarizes the dielectric material, in such a way that the negative charges in the material orient themselves toward the positive electrode and the positive charges toward the negative one. Because the charges in an insulator are not free to move, the polarization effect that opposes the applied field attracts charges onto the electrodes

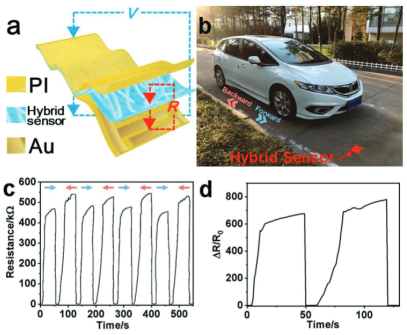

Figure 1.7: hybrid aerogel/hydrogel piezoresistance sensor with high upper pressure range limit [11]

and stores energy in the capacitor.
Piezocapacitive pressure sensors detect an external pressure through a change in electrical capacitance, which is defined as:

$$C = \epsilon \frac{A}{d} \tag{1.4}$$

where ϵ is the dielectric permittivity, A is the overlapping area of the armatures and d the distance between them.
In particular $\epsilon = \epsilon_r \epsilon_0$, with ϵ_0 permittivity of air and ϵ_r relative dielectric permittivity of the material.
Sensitivity for these sensors, similarly to piezoresistance-based ones, is given by:

$$S = \frac{\frac{\Delta C}{C_0}}{\Delta X} \tag{1.5}$$

Fabrication techniques aimed at increasing the performance of these sensors include porous and surface microstructures [13] and can be employed both for the electrodes or for the dielectric layer. Porous structures have the ability to increase the relative dielectric constant variation, while surface microstructures are commonly used with the aim to the maximize the variation of interface (term A in eq.(1.5)) between the layers with pressure. This in turn translates to an higher capacitance variation.
On this note, Su et al.[14] prepared a microstructured PDMS layer by drop-coating the mixture onto 3D-printed metal mold with different microstructures (hemispheres, cones, truncated cones). FEM simulation was used to measure the displacement of the microstructures varying their height (Figure 1.8). The hemisphere microstructure on PDMS substrate was found to be the most sensitive in piezocapactive mode and used to build a sensor to monitor finger bending and plantar pressure.
Regarding the use of porous structures, Zhong et al. [15] instead, developed a flexible capacitive pressure sensor through the use of a high concentration CNT-doped

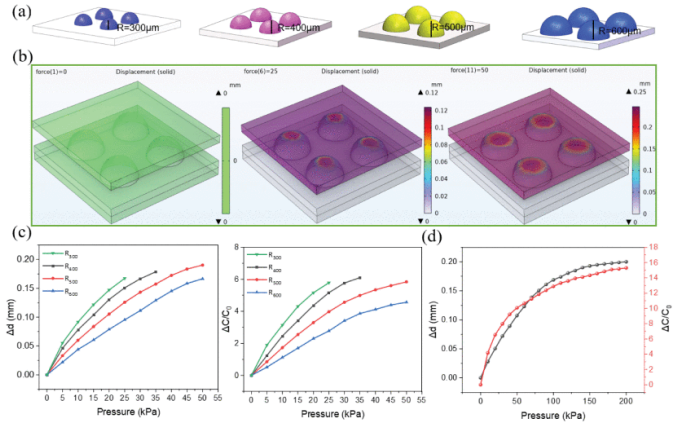

Figure 1.8: FEM simulation and performance of microstructures patterned on a flexible PDMS dielectric layer for use in a piezocapacitive sensor [14]

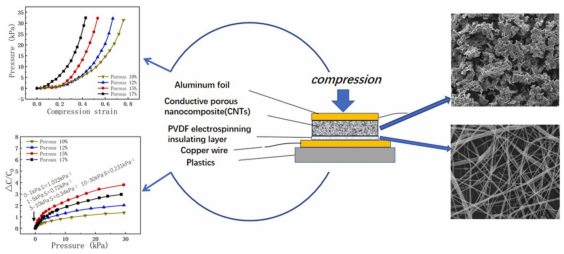

Figure 1.9: Porous electrode capacitive pressure sensor [15]

porous electrode and an ultrathin porous PVDF dielectric layer, with an aluminum foil as the other electrode (Figure 1.9). The sensor exhibited high sensitivity, fast response and cyclic stability and was employed to monitor physiological signals, demonstrating its potential for healthcare applications.
Sensors designed with this kind of transduction mechanism in mind are capable of static and dynamic pressure measurements, but have the drawback of being easily influenced by external noise, since charges accumulated on the capacitor plates can be easily affected by surface charges of other objects. This problem can also be turned into a opportunity to achieve non-contact sensing, as in [16].
Moreover, the capacitance change requires an external power source to be measured (similarly to piezoresistance devices).

1.2.3 Triboelectric sensors

Triboelectric sensors work on the principle of electric charge transfer between two materials colliding when subjected to repeated contact or sliding forces. This periodic movement causes an accumulation of opposite charges on the two layers

and thus a potential difference. A current is then produced if the two layers are connected through an external circuit.
Evaluating the effectiveness of a material for triboelectric application means taking into account the triboelectric series, an empirical collection of materials sorted by their ability to acquire positive or negative charge. Ideally, materials far apart along the series are chosen for maximum electrical output. On this note, recent studies [17], [18] have shown that hard polymers/rough surfaces tend to acquire a positive surface charge, whereas soft polymers/ smooth surfaces are negatively charged.
The material is not the only thing that has to be considered: velocity and force of the collision, as well as local roughness and strain between the two materials are some of the main parameters affecting the response of these sensors [19].
Triboelectric sensors offer an additional design choice: their mode of operation 1.10]. They can be operated in contact separation mode, lateral sliding mode, single electrode mode and freestanding triboelectric-layer mode.
The vertical contact separation mode is the easieast to implement: triboelectric layers come into contact from the vertical direction and charges are accumulated on their surface. As the layers are separated by an air gap, they produce a potential difference and a current flowing in the load. The current produced is usally an alternating one, but recently Shi et al. [20] investigated a contact separation mode TENG made with poly(thioctic acid) (PTA) adhesive as one of the layers. The use of an adhesive and conductive interface as the two TENG (TriboElectric NanoGenerator) layers provided charge dissipation, which produced a DC output. [Figure 1.11]

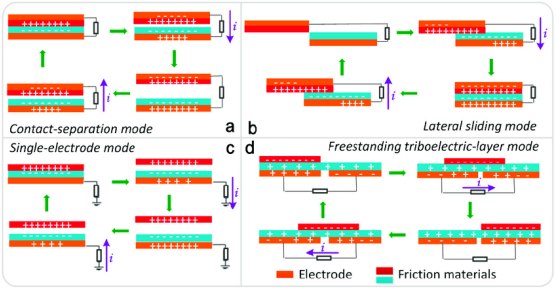

Figure 1.10: Working modes of TENGs [21]

The lateral sliding mode is similar to the previous, but in this case the contact happens in the horizontal direction.
The single electrode mode has the dielectric layer free to move and one of the electrodes grounded, which makes these sensors easy to operate and to be integrated. This mode of operation is also preferred if human skin is to be used as one of the triboelectric layers [22].

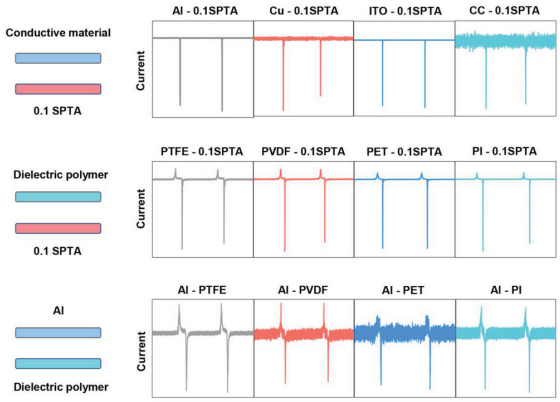

Figure 1.11: Conductive-adhesive interface (top) in PTA-based TENG able to provide a DC output [20]

The freestanding-triboelectric mode works with a moving dielectric layer between electrodes. In contrast to contact mode, freestanding mode avoids the electrostatic shielding effect, thus being able to achieve higher efficiency in charge transfer through external circuits [23].

The main benefit of exploiting the triboelectric effect are the self-powering ability of the device, allowing them to be useful for low-grade energy harvesting in the most diverse situations. For example, Yu et al. [24] were able to fabricate a flexible TENG with flame-retardant capabilities. The device was built by impregnating a cotton-ammonia based fabric into PPy (Polypyrrole), a commonly used electrode for triboelectric applications, and subsequently into a chitosan/phytic acid solution to enhance the binding efficiency of electrons and provide flame retardant capabilities. The device built was almost completely biodegradable after 100 days, had excellent air/moisture permeability and decently stable voltage generation after being exposed to fire. The alternating current produced was rectified and used to power a LED.

Lastly, some of the drawbacks of this transduction mechanism are the inability to perform static measurements and the degradation of electrical signal due to friction heat generated between the contact layers (especially in the lateral sliding mode). The high sensitivity to environmental humidity of some of the biocompatible materials (such as natural fibers) used as triboelectric layer is also problematic, since evaporation of water molecules tends to neutralize the triboelectric charge [25]
.

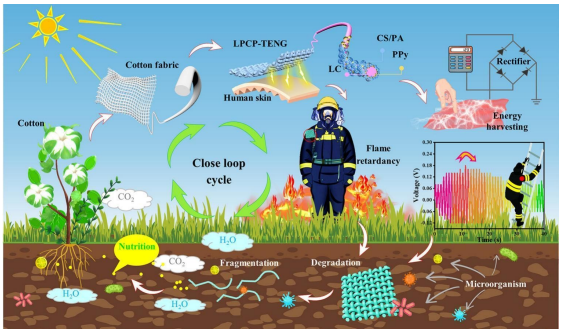

Figure 1.12: Cotton-based biodegradable and flame retardant TENG [24]

1.3 Piezoionic sensors

1.3.1 The piezoionic effect

Piezoionics is a relatively new field of study which has attracted attention due to its promising capabilities in providing bio-inspired mechanical to electrical transduction and energy harvesting abilities.
The phenomenon concerns the creation of a voltage difference as a result of a displacement of ions inside the electrolyte of a polymeric material.This rearrangement of ionic species is exerted by external stress, which produces an hydrodynamic drag force. The difference in mobility plays a pivotal role in the separation of the ions and in the creation of an electrical potential difference over time.[26]

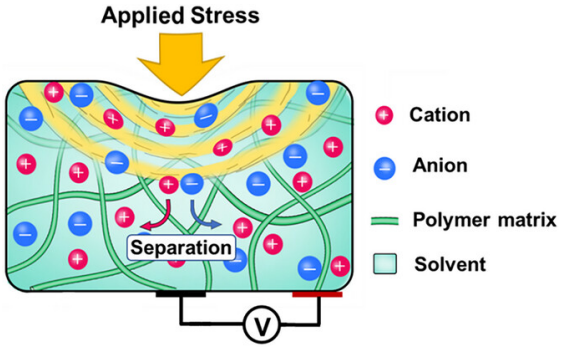

Figure 1.13: Piezoionic effect mechanism [26]

As with the piezoelectric effect, the inverse mechanism has also been observed: the application of a voltage difference to the material, by inducing a movement of ions inside the electrolyte, creates a pressure difference which is able to induce a displacement of the polymeric matrix measurable as a strain difference.

In the experiment set up by Whoeling et al.[27], a NBR (nitrile butadiene rubber) network was sandwiched between two electrically conductive polymer (ECP) layers. The application of a voltage leads to oxidation of the working electrode, whose charges are balenced by either anions or cations in the electrolyte swollen NBR. This brings about either an expansion or a contraction of the electrode, according to which of the ions is more mobile. Changing the solvent also influences the diffusivity of the ions.

The physical modeling of the piezoionic effect involves coupling mechanics, fluid flow, poroelasticity and electricity generation. It all starts from the conservation of mass equation in a fluid (Nernst-Planck equation):

$$\frac{\delta c^k}{\delta t} + c^k \nabla \cdot v_s + \nabla \cdot J_k = 0 \tag{1.6}$$

with c_k concentration of the species k, v_s velocity of the polymer network and J_k the mass flux to which the k species is subjected.
It is possible to write J_k as summation of three different flows:

- the advective flow, which describes the transport of a substance by the bulk fluid motion and in the present case concerns the fluid flow through a porous medium (in our case an hydrogel matrix) thanks to the Darcy law:

$$J_{adv,k} = -\beta_k \frac{\kappa}{\mu} \nabla P \tag{1.7}$$

  (with κ hydrogel permeability, μ fluid viscosity and β_k hindrance factor of the k ion). The hindrance factor is particularly important, and correlates the mobile ion(s)' size with the porosity ϕ of the matrix [28]. Differences in hindrance factors translate in difference in mobilities of the ions.

- the diffusion flow, governed by Fick's law:

$$J_{diff,k} = -D_k \nabla c_k \tag{1.8}$$

  with D_k diffusivity of the k ion.

- the electromigration flow, which brings on the creation of an electric potential

$$J_{e,k} = c_k \frac{D_k z_k e}{k_B T} \nabla \psi \tag{1.9}$$

  with z_k number of charges of the k ion, e elementary charge, K_B Boltzmann constant, T absolute temperature and ψ electrostatic potential.

The conservation of momentum and poroelastic model complete this picture.
The interplay between Darcy and diffusion flow creates a convective flux. Once convection ends, equilibrium is restored and a decay in sense voltage is observed [27].
Empirically, it has been found that a Donnan equilibrium model can relate the behaviour of the piezoionic voltage at small compressive strains [29]. This phenomenon arises when charged particles are not distributed homogeneously on the two sides of a cell's membrane and ions are attracted/repulsed based on their ability to cross the barrier. The equation proposed by Odent et al. (a rielaboration of the Donnan potential one) is:

$$\Delta V_{Donnan} = \frac{kT}{e} ln \frac{C_{indent}}{C_{bulk}} \tag{1.10}$$

where $C_{indent} = (1 - \epsilon)C_{bulk}$, with ϵ compressive strain, C_{indent} and C_{bulk} concentration of immobile ions under the indenter and in the bulk electrolyte respectively. By analizing the slope of the strain-voltage curve, the group was able to confirm the Donnan model picture.

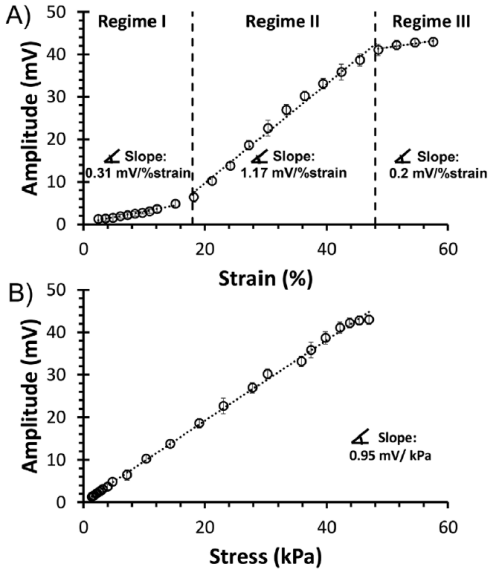

Figure 1.14: Piezoionic voltage relation to compressive strain (top) and compressive stress (bottom) [29]

A streaming potential model is able to model the response across a wide range of compressive stresses (Figure 1.14). According to the equation derived by Dobashi et al. [30], this translates to:

$$\Delta V = -\frac{eN\kappa}{\sigma\mu}\left[\frac{D_+}{D_{0+}} - \frac{D_-}{D_0}\right]\Delta P = \alpha\Delta P \tag{1.11}$$

Here, the two diffusion coefficients D_O take into account the ions' interaction with the polymeric matrix. The piezoionic coefficient α directly relates the voltage produced to the pressure variation and can be increased by increasing the difference in the ions' diffusivities or tuning either viscosity of the solvent or permeability of the polymeric matrix.

1.3.2 State of the art and application of piezoionic sensors

Research advancements in the piezoionics field can bring benefits in multiple fields, from sensors monitoring human physiological signals, to human-machine interfaces and energy harvesting devices.

Sensors based on the piezoionic effect offer high sensitivity to dynamic stimuli utilizing flexible materials, differently from those based on crystalline piezoelectric materials. The ability to detect static forces [31] and to provide an intrinsic DC output is also a major benefit with respect to TENGs.
The piezoionic effect is also not dependent on contact area change, which is usually a main aspect of capacitive pressure sensor. Interfacial effects still play a major role: it is important to reduce degradation of the signal by avoiding modulus mismatch of the electrodes with the polymer, as Lu et al. [32] did by seeding metal ions in a polyelectrolyte and growing an electrode by chemical reduction (Figure 1.15.

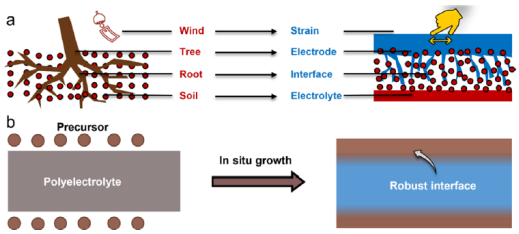

Figure 1.15: Bio-inspired polyelectrolyte-electrode interface optimization [32]

Piezoionic sensors offer the ability to detect a wide variety of body movements, as demonstrated by [33] et al, which developed PressION, an all-fabric based sensor, by treating cotton with a siloxane based polymer containing free anions in solution. The device was able to recognize phonation signals, knee/elbow joint movement and pressure exerted by a foot when placed in an insole (Figure 1.16).

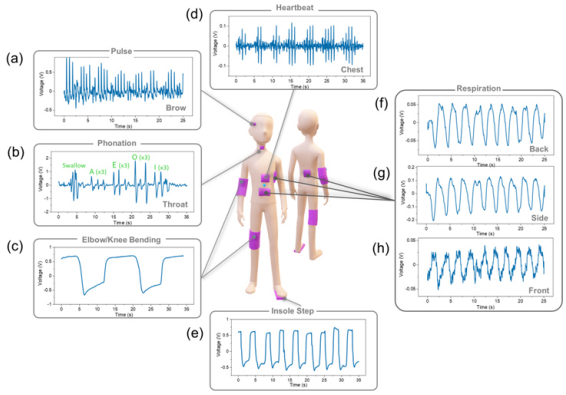

Figure 1.16: All-fabric piezoionic sensor able to detect multiple physiological signals [32]

On the topic of biointerfaces, the high charge density able to be output by piezoionic devices can be used for nerve simulation, as demonstrated by Dobashi et al. [30], which fabricated an array of acrylic acid (AA) hemispheres surrounded by pAAm. They were able to reproduce a resting negative potential of -50mV (by tuning the AA content) which became more negative under pressure applied. The array was connected to the sciatic nerve of a mice and, through signal amplification, limb twitches were detected (Figure 1.17)

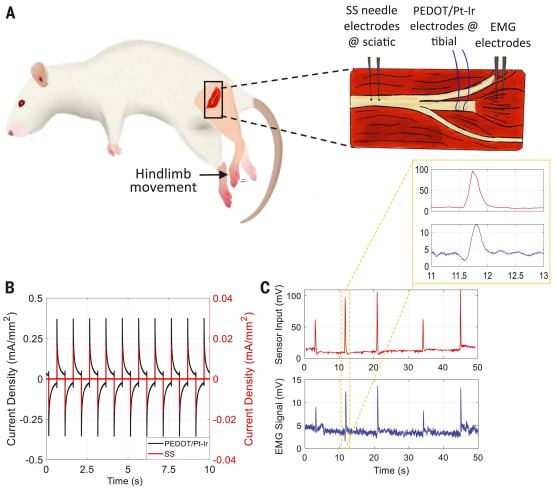

Figure 1.17: Peripheral nerve stimulation in mice through piezoionic phenomenon [30]

Future advancements in the development of piezoionic sensors include the ability to scale up and optimize the production using accessible and highly tunable methods.

On this note, Smith-Jones et al. [34] were recently able to fabricate modular piezoionic sensors based on ionic liquid via 3d printing. The various printed shapes could be joined together in a loop or a cube by heating the samples. Tensile stretch applied to the loop showed a decrease in current, while compressive stress on the cube increased the piezoionic response.

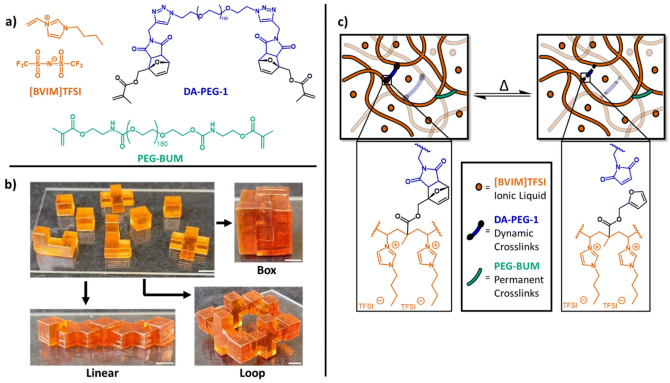

Figure 1.18: Composition of the resin (a,c) and printed piezoionic modular samples (b) [34]

.

The ability to enhance the signal generated by tailoring the ionic species and their interplay with the polymeric matrix, together with the self-powering abilities and bio-inspired transduction mechanism certainly make the piezoionic effect worth of additional research.

Chapter 2

Materials and methods

2.1 DLP 3D-printed cellulose samples

The cellulose samples measured were composed of:

- 51.81% wt. acrylic acid (AAc), a widely used monomer in 3d-printing, notable for its fast polymerization rate;
- 6.02% wt. microcrystalline cellulose (MCC), a green additive which offers water retention and improved mechanical and rheological properties, in addition to enhanced matrix porosity due to its large surface area [35];
- 4.82% wt. water;
- 37.35% wt. zinc chloride ($ZnCl_2$), binary salt used to provide ionic conductivity to the neutral matrix

The samples were 3D-printed through Digital Light Processing (DLP), an additive manifacturing technique in which a light beam emitted by a projector cures a liquid resin one layer at a time.

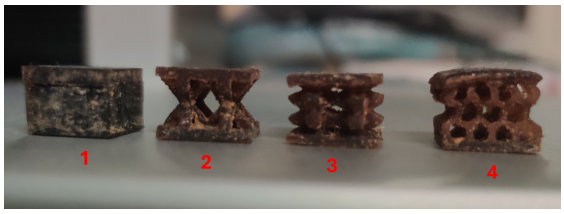

Figure 2.1: 3d-printed cellulose samples: 1) cube 2) star 3) tristar 4) honeycomb

These samples were measured to determine which geometry would produce the highest electrical response. An alternative method to produce a piezoionic voltage

by exploiting a charged matrix was then investigated through a ionic liquid-based conductive polymer.

2.2 Ionic liquid sample components

2.2.1 Ionic liquid

Ionic liquids are a class of organic compounds whose chemical structure is composed of a bulky cation and a smaller anion.
These salts possess various interesting abilities: their low tendency to evaporate and thermal stability allows them to be used as green solvents, even for organic reactions at high temperature. Their wide electrochemical window, on the other hand, makes them suitable candidates as electrolytes in batteries. Ionic liquids have also been reported to enhance the conductivity of polymer electrolytes [36] by rendering part of the matrix amorphous and favoring ion movement.
A particular class of ionic liquids is the one of polymerized ionic liquids (PIL) [37], which combine the thoughness and tunable elastic properties of polymers with all the previous capabilities of ionic liquids, while providing intrisinc conductivity. This ionic polymers can however have lower ion diffusivities than their liquid counterparts [38].

The ionic liquid used in this work is a [2-(Methacryloyloxy)ethyl]trimethylammonium chloride solution (Figure 2.1) (Sigma-Aldrich), which comes as 75% wt. in water. It is monofunctional and it has been notably used to provide cationic conductivity to polymers [39], to enhance the antimicrobial properties of adhesives [40] and to prevent cell growth on polymide (Kapton) [41].

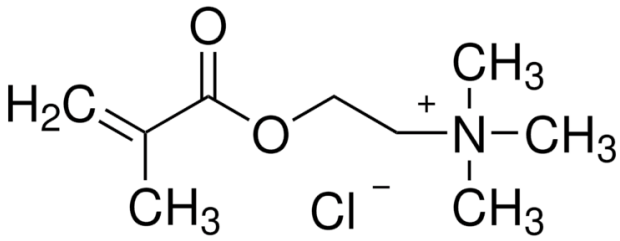

Figure 2.2: [2-(Methacryloyloxy)ethyl]trimethylammonium chloride solution , the ionic liquid used in the formulation.

A polymerized ionic liquid has been chosen to investigate how the piezoionic effect develops when the polymeric matrix is charged and a single counterion is present in solution.

2.2.2 PEGDA

Polyetilene Glygol Diacrylate (PEGDA, average molecular weight 700 g/mol, purchased from Sigma-Aldrich) has been used as crosslinker, to improve the mechanical properties of the PIL. A low concentration (2% v/V) has been chosen to avoid the structure from becoming too rigid. At higher concentrations, the samples had lower elongation at break and exhibited a lesser homogeneous structure when stretched, due to more adjacent chains binding together.

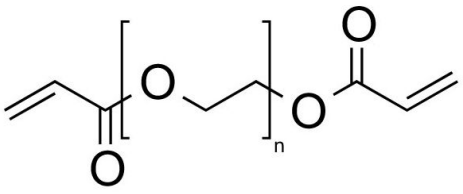

Figure 2.3: Polyethylene glycol diacrylate, used as crosslinker in the formulation

.

2.2.3 Glycerol

Glycerol is an organic compound containing three hydroxil (-OH) groups. Its ability to form hydrogen bonds with water can lead to lower evaporation rates of the glycerol-water mixture, which decrease as glycerol concentration increases.
As an humectant, glycerol tends to retain moisture from the environment, a trend which once again increases linearly with the triol's concentration in solution [42].

In the present work, glycerol has been used mainly as a plasticizer [43], to increase the free volume within the matrix. The initial samples tested, containing no glycerol, were deemed too brittle, which might be due to the fact that the methacrylate group in the PIL has been shown to lead to harder structures than e.g. ionic liquids containing an acrylate group [44].

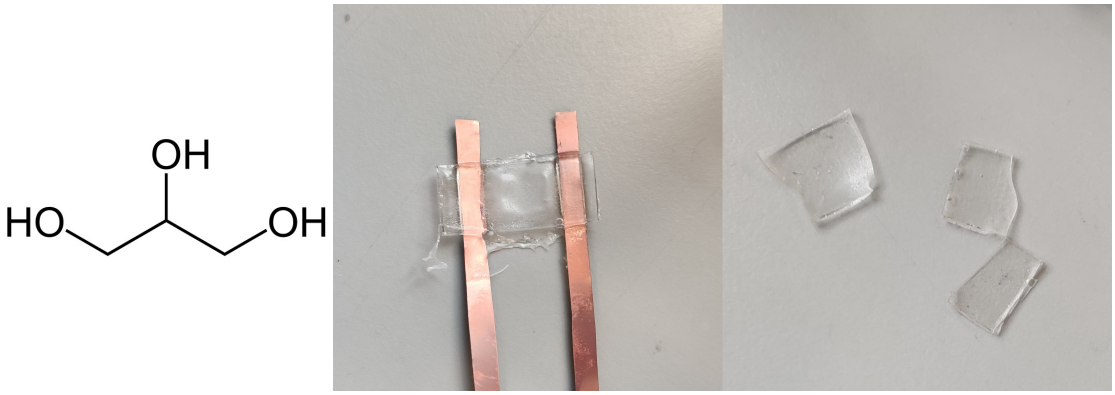

Figure 2.4: Glycerol (left) and brittle containing only the ionic liquid, the crosslinker and photoinitiator (right)

A low amount of glycerol has been found to increase the tensile strength and elongation at break of the sample, while higher concentrations exhibit an opposite trend for these two properties while at the same time conferring an higher degree of elasticity.

2.2.4 TPO-SDS

Diphenyl(2,4,6-trimethylbenzoyl)phosphine oxide (TPO) has been used as photoinitiator. This molecule undergoes cleaving into two radical species under UV light irradiation and the reactive compounds formed initiate the polymerization. The reaction byproducts are usually incorporated in the matrix once the chain growth is terminated.
Normally insoluble in water, the TPO utilized in this work contains Sodium Dodecyl sulfate (SDS), an anionic surfactant which allows the powdery nanoparticles to be dissolved in a liquid solution.

2.3 Formulation preparation

The formulation tested were two. The glycerol amount as volume fraction was fixed as either 10% or 30%, the PEGDA-700 volume fraction as 2% and the photoinitiator as 1% weight fraction with respect to the ionic liquid monomer.
The conversion from volume fraction to weight fraction was obtained through the density of the components.

The weighting of components was done on a precision scale. The ionic liquid was weighted first, then PEGDA-700 and glycerol were pipetted in the vial.

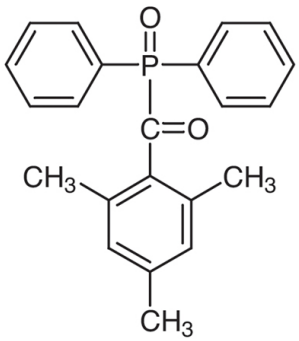

Figure 2.5: Diphenyl(2,4,6-trimethylbenzoyl)phosphine oxide, the photoinitiator used

.

Component	Density
MAETAC ionic liquid	1.105 g/mL [45]
PEGDA-700	1.12 g/mL [46]
Glycerol	1.25 g/mL [47]

Table 2.1: Density of the components in the formulation

The TPO photonitiator powder was added after wrapping the container in aluminum foil to avoid a possible premature visible light-induced polymerization reaction. The formulation was then mixed in a magnetic stirrer equipped with a hot plate at a temperature of 50°C and 300 RPM for approximately 20 minutes.

2.4 Ionic liquid sample preparation

The samples were prepared by pouring the formulation in polydimethylsiloxane (PDMS) molds.
Two configuration were tested: a dogbone-shaped one and a square with area 1cm x 1cm and thickness determined by the amount of formulation drop casted.

The photopolymerization was achieved though a Hamamatsu LC8 Lamp, with an intensity of 35 mW/cm^2. A small chamber allowed to carry on the reaction in a controlled environment. The chamber's glass was made of quartz (material with a very low UV absorbance) and was equipped with an inlet through which gaseous N_2 could be fluxed. Nitrogen was necessary to avoid oxygen inhibition, which terminates the reaction prematurely. The gas was dispersed at a pressure of 1 bar on the mould for about 30 seconds before turning the lamp on and exposing the sample for 8 minutes on one side.

Formulation	MAETAC vol. fraction	Glycerol vol. fraction	PEGDA-700 vol. fraction
10gly2peg	88% v/v	10% v/v	2% v/v
30gly2peg	68% v/v	30% v/v	2% v/v

Table 2.2: Volume fraction of liquid components in the formulation

Formulation	Glycerol wt. fraction	PEGDA-700 wt. fraction	TPO wt. fraction
10gly2peg	13% wt.	2.34% wt.	1% wt.
30gly2peg	50% wt.	2.98% wt.	1% wt.

Table 2.3: Weight fraction of components with respect to the ionic liquid

Figure 2.6: Formulation before (left) and after (right) being mixed in the magnetic stirrer

The sample was then flipped and Cu-Kapton electrodes (with an area of 0.5mm x 40mm) were attached with a drop of formulation. The irradiation process was then repeated for additional 8 minutes on the other side.

Figure 2.7: Sample photopolymerization setup

.

Figure 2.8: Dogbone (left) and square (right) sample of the ionic-liquid based polymer

2.5 Characterization of the samples

2.5.1 Mechanical characterization

The mechanical characterization was performed with an Instron Z5 tensile tester, coupled with the software THSSD. The data obtained was post-processed with Origin (OriginLab Corporation).
The dogbone sample was first measured with a digital caliper (LinearTools ©) and its cross-sectional area determined at midpoint.
The sample was then secured between the machine grips and the starting length l_0 measured as the distance between the grips. The load cell's measured force and position were then reset and the needed displacement configured in the software.

The samples were either:

- stretched until rupture at a speed of 5 mm/min in the breaking tests

- stretched cyclically until 100% strain at a speed of 10 mm/min to evaluate the mechanical hysteresis
- stretched until 25% strain at a speed of 5 mm/min in the durability tests

In the durability tests, the temperature T and relative humidity RH were recorded through a BME280 mounted on a breadboard and controlled through and Arduino Uno microcontroller. The readout was performed with the aid of the related Arduino IDE.

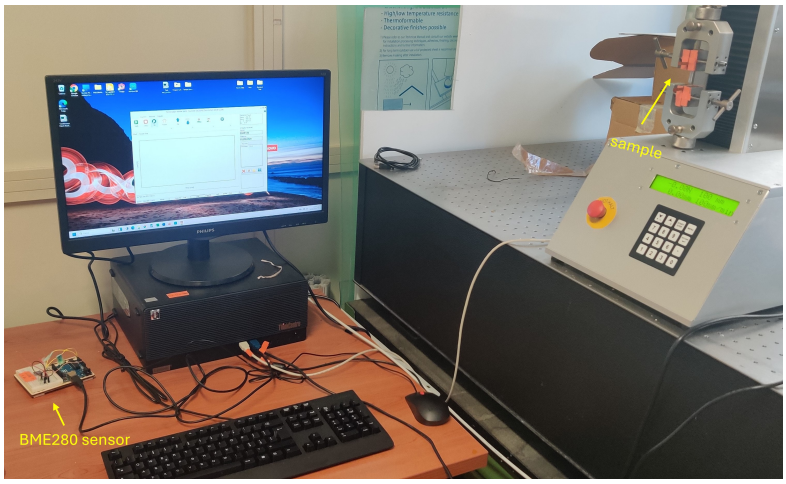

Figure 2.9: Mechanical characterization setup

.

From the resulting data, the strain was calculated as:

$$\epsilon = \frac{\Delta L}{l_0} \tag{2.1}$$

with ΔL the load cell course during the test, starting from zero position.
The tensile stress was calculated as:

$$\sigma = \frac{F}{A} \tag{2.2}$$

with F the force measured by the load cell and A the sample cross sectional area.

The Young Modulus was calculated by fitting the elastic deformation region of the stress-strain curve, which has been considered as the initial part up to 5% strain experienced. After this point most polymeric material will experience a plastic behavior.

$$E = \frac{\sigma}{\epsilon} \tag{2.3}$$

The elastic modulus is the slope obtained through the fit.

The tensile strength and elongation at break have been taken as the maximum tensile stress before rupture and its corresponding strain point, respectively.

2.5.2 Electromechanical characterization

The electromechanical characterization was performed by coupling the Z5 tensile tester with a Keithley 2440 multimeter. The electrical signal data acquisition was performed through LabView (National instruments) and the results post-processed though the aforementioned Origin software.

In the dogbone configuration, the sample was placed on a metal plate insulated with polymide and held firm with additional tape.
The electrodes were then connected to the multimeter through crocodile clips 10 loading/unloading cycles were programmed through the THSSD program. The sample was compressed through a 3d printed indenter with an area of 1cm x 1cm placed on the top grip. Two crosshead's speeds were chosen, 20 mm/min and 50 mm/min, to investigate if the rate at which pressure is applied influences the ion separation magnitude and thus the response produced.
In the graphs, the pressure reported is calculated dividing the force applied by the area of the indenter, equal to 1 cm^2.

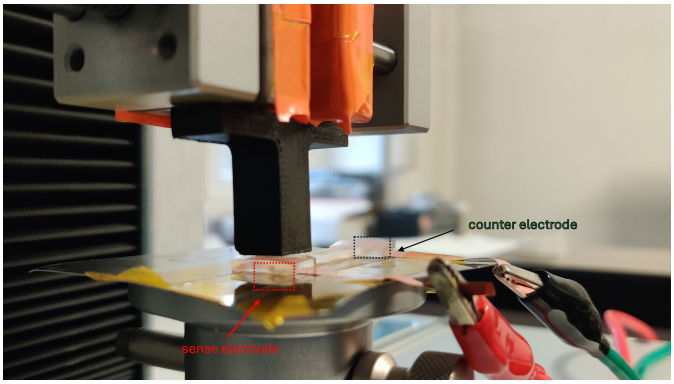

Figure 2.10: Dogbone electromechanical characterization setup

.

In the square/sandwich configuration 2.11, the top grip was replaced by a metal plate. Electrodes were placed on the top and bottom plates, and insulated with

Kapton tape, leaving space for the sample. After connecting the Cu-polymide electrodes to the multimeter, the piezoionic response was recorded performing 10 cycles in this case as well. The preload setting, in this case, was adjusted for each test in order to account for the non perfect uniformity of the sample surface. In this way, the top plate could remain attached to the sample during the test.
Also in this case the test velocity of the crosshead was 20 mm/min and 50 mm/min and the pressure reported in the graphs is obtained by dividing the force applied by the cross sectional area of the samples, which is 1 cm^2.

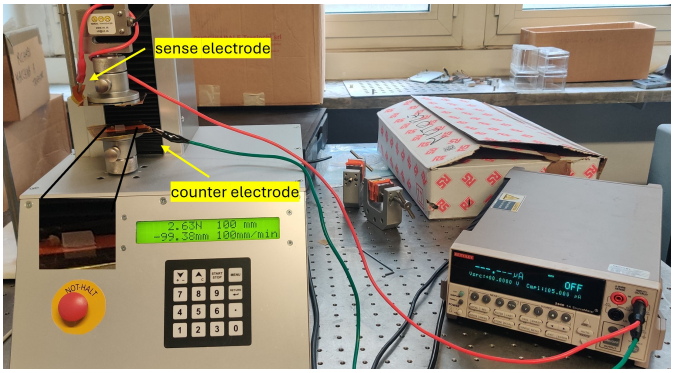

Figure 2.11: Square electromechanical characterization setup

.

The setup just described is the same used for the characterization of the 3d samples and is reported in fig. 2.12

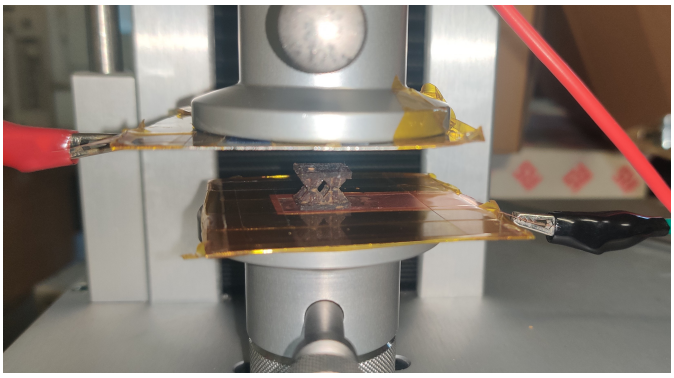

Figure 2.12: DLP printed cellulose sample electromechanical characterization setup (star sample pictured here)

.

Chapter 3

Results

3.1 Piezoionic response of 3D-printed cellulose samples

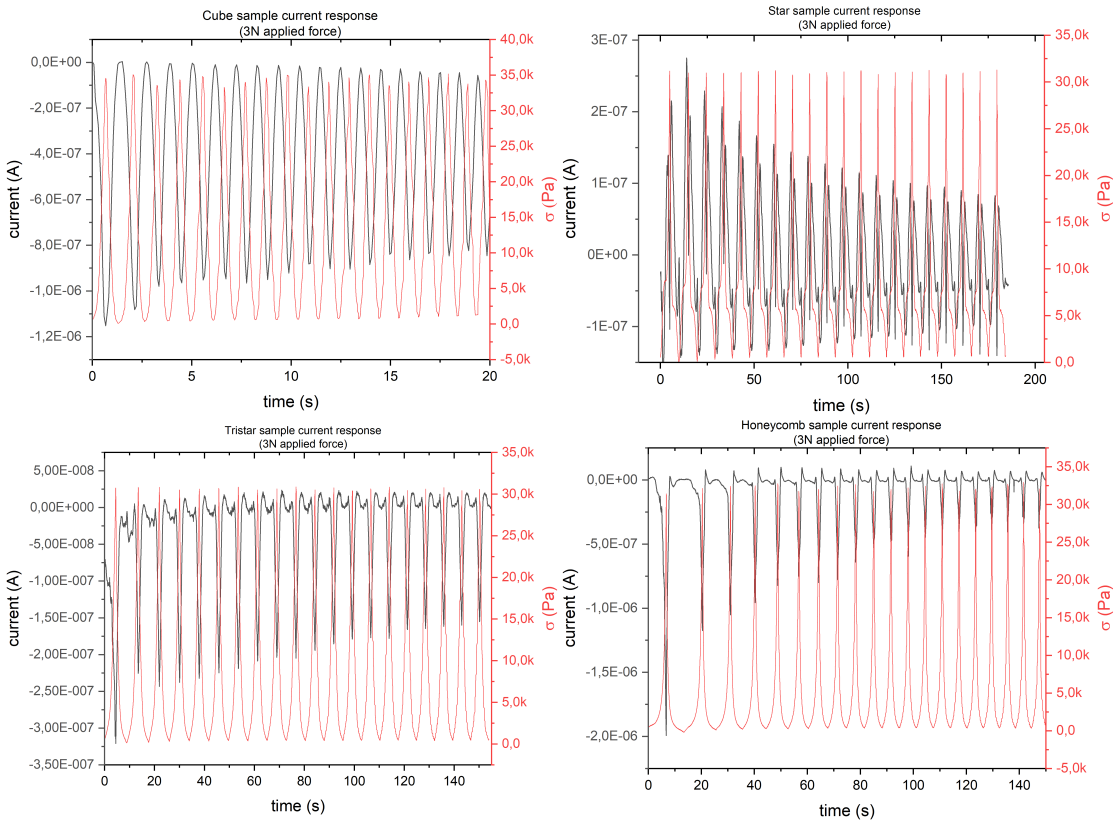

Figure 3.1: Current response to 20 loading-unloading cycles at a force of 3N of: cube sample (top left), star sample (top right), tristar sample (bottom left), honeycomb sample (bottom right).

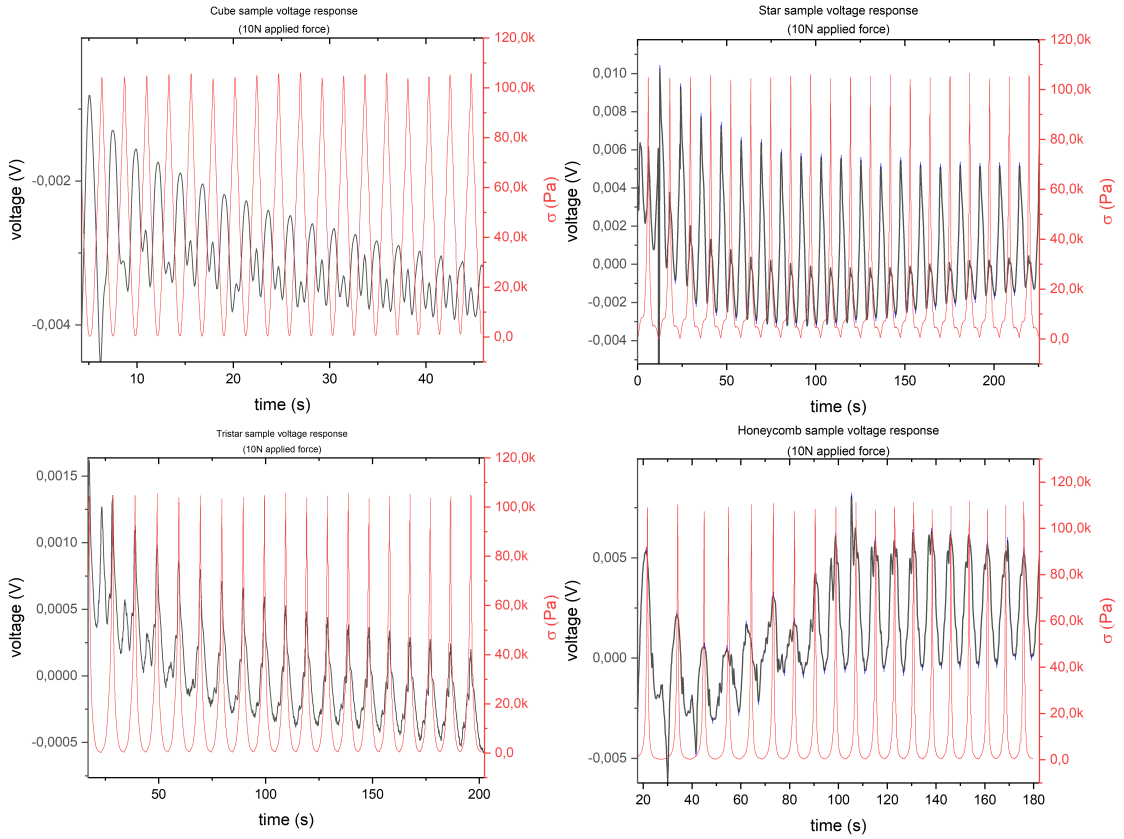

Figure 3.2: Voltage response to a 10N loading-unloading cycle of: cube sample (top left), star sample (top right), tristar sample (bottom left), honeycomb sample (bottom right)

The current response of the samples is shown in figure 3.1. The waveforms produced tend to be mostly similar, apart from the one of the star structure on the top right. The geometry influences the amount of current decay experienced, which is lower in the cube and higher in the honeycomb sample.

The voltage response to 20 loading-unloading cycles on the 3d-printed samples at a pressure of 100 kPa is shown in fig 3.2.
The voltage waveform seem to in general be less stable, but the positive peaks confirm the displacement of the Cl^- ions away from the pressure site (and the sense electrode) and towards the reference electrode. The star sample in particular shows higher voltage peaks which are synchronized with the force removal (top left figure in fig. 3.2) and it may be due to the fact that this particular geometry relaxes in a short amount of time, producing an high pressure gradient (eq.1.11) as soon as the force is removed.

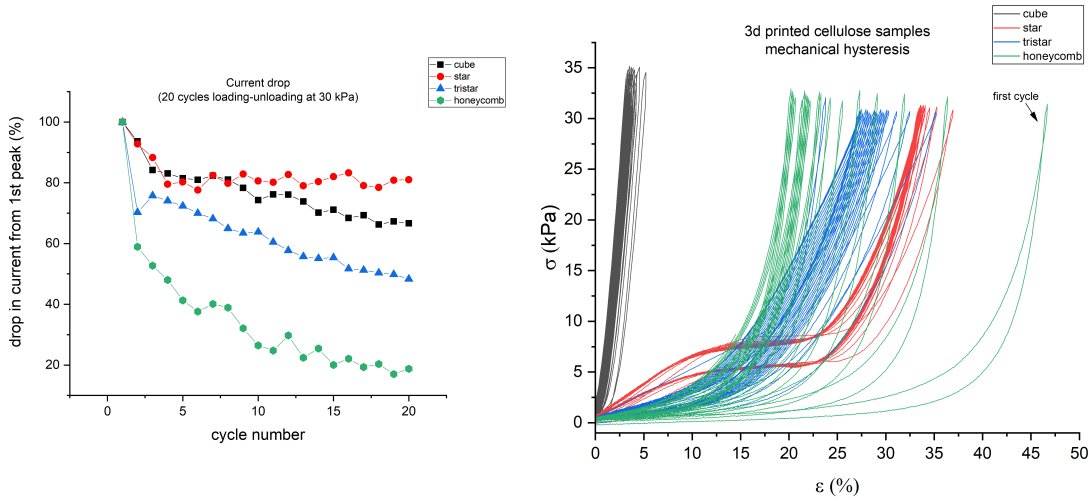

Figure 3.3: (left) current drop vs number of cycles (right) mechanical hysteresis curves of 3d samples. The pressure applied is 30 kPa in both cases

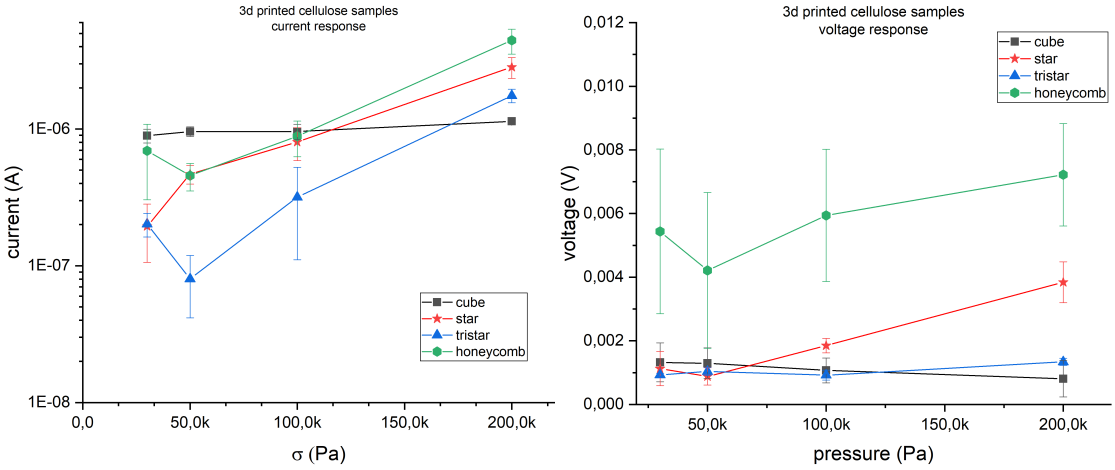

Figure 3.4: (left) current and (right) voltage response to different pressures, taken as peak-to-peak value

In figure 3.3 (left) it is once again possible to appreciate the larger current drop after the first cycle experienced by the honeycomb sample.
On the right, the dynamic stress-strain curves are reported. The cube, as expected, experiences the lowest maximum deformation but has a very low loss of signal due to the geometrical structure rigidity. This means that the solvent flow carrying the ions experiences the least amount of obastacles in its path.
The honeycomb sample undergoes the highest maximum compressive strain in the first cycle but tends to deform less afterwards. The star sample shows the highest

hysteresis and a high pressure gradient towards the end of the loading cycle.

Finally, in figure 3.4 the average peak-to-peak voltage and current produced are reported. Each point in the graph is taken as the response of the sample at a particular pressure, averaging the peak-to-peak values across the 20 cycles performed, including the first cycle (which is the one generating the highest response). The error bars represent the standard deviation about the average, which is usually larger if the sample has an unstable waveform.
From this graph, the honeycomb sample seems to be the best performing, especially at higher pressure stimuli where it is capable of deforming more with respect to the others.

3.2 Ionic liquid based sensor

3.2.1 Tensile tests - evaluation of mechanical properties

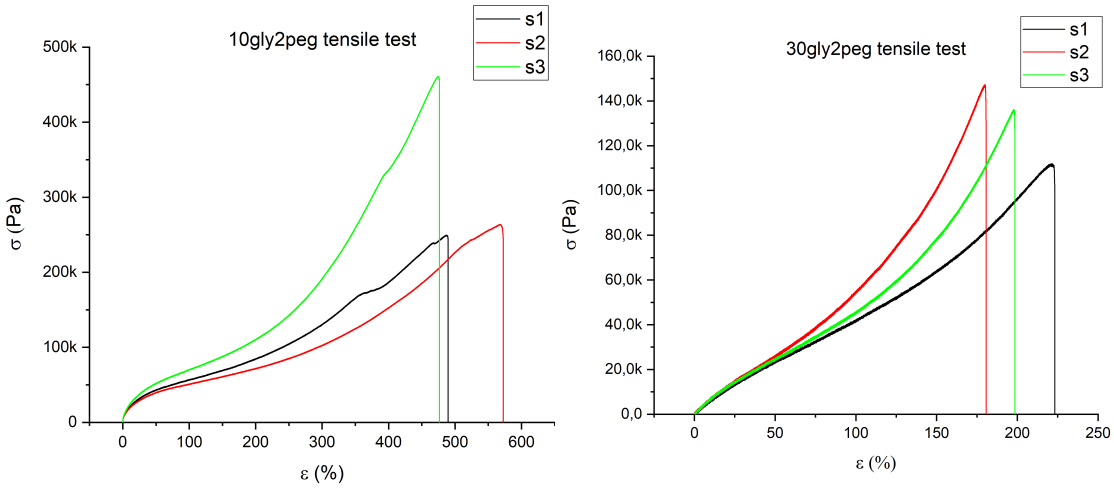

Figure 3.5: (left) 10gly2peg rupture tests and (right) 30gly2peg rupture tests

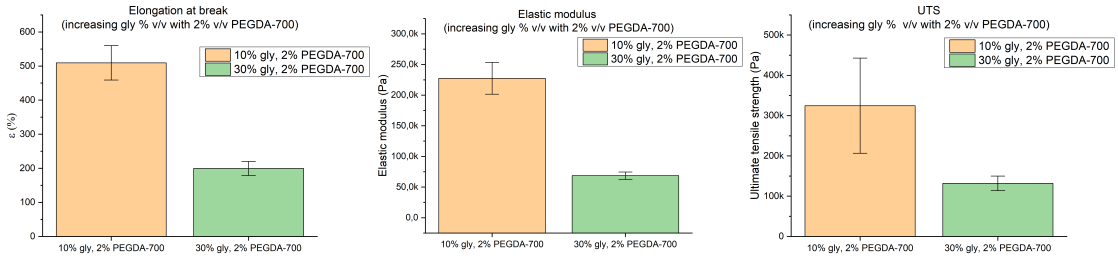

Figure 3.6: (left) elongation at break (mid) elastic modulus (right) tensile strength of the samples

As it can be seen from the graphs in fig. 3.6, the increase of glycerol in solution tends to decrease the final elongation reached by the sample but at the same time it produces a softer material, as the lower elastic modulus suggests. This is a behaviour commonly found in literature [48] [49], as the -OH groups in the glycerol's chain may tend to reduce the attractive forces between the ionic liquid's polymeric chains, facilitating their mobility. Additionally, crosslinking density is generally lower, which might partly explain the stickyness of the samples with high glycerol concentrations.
Samples prepared with the two formulation were subjected to cyclical tensile tests, as depicted in fig. 3.7.

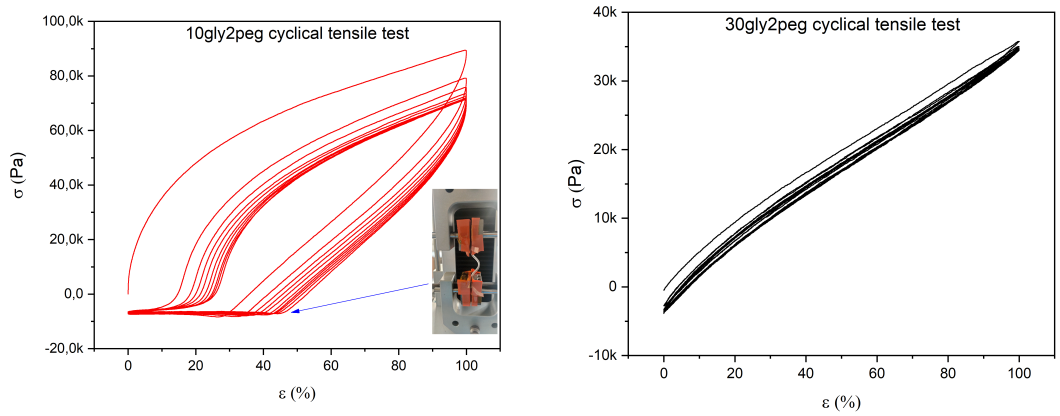

Figure 3.7: (left) 10gly2peg and (right) 30gly2peg cyclic tensile test

The 10gly2peg formulation, which was more rigid, exhibited a viscoplastic behavior, with residual strain accumulating in the material at each cycle. The picture in the inset shows the end of one of the unloading cycles, with the permanent deformation clearly visible.
Samples using the 30gly2peg formulation, on the other hand, posses a viscoelastic behaviour with a very low hysteresis loss after each cycle.
In figure 3.8 it is possible to better appreciate the hysteresis reduction due to increasing glycerol content in the formulation.

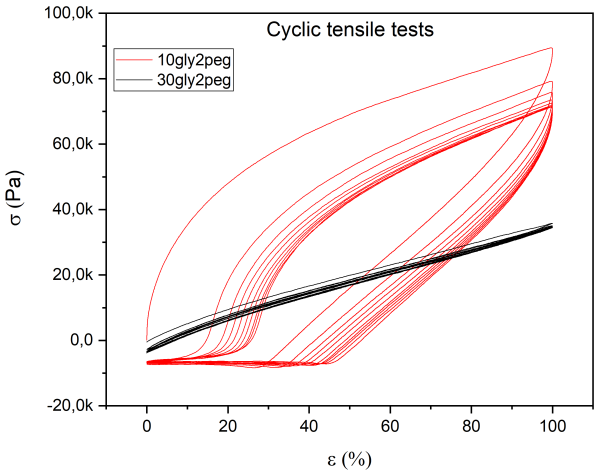

Figure 3.8: Cyclic tensile tests of samples using the two formulations

.

3.2.2 Durability tests

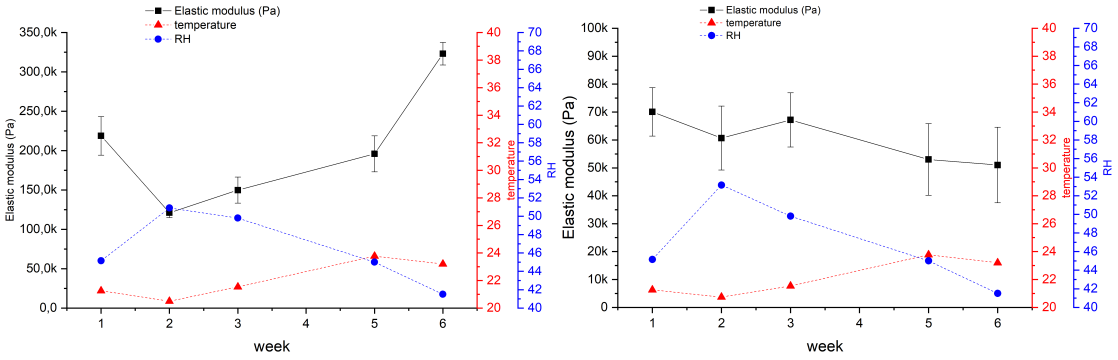

Figure 3.9: (left) 10gly2peg durability test (right) 30gly2peg durability test

The elastic modulus durability tests carried out are hereby reported. For the purpose of the trial, the samples were stored in a petri dish at ambient conditions. The temperature and RH reported here are the ones recorded when the measurement was performed. The elastic modulus value is the mean between the one obtained by three different samples, with relative standard deviation.

It is possible to notice a more marked dependence of the elastic modulus on the ambient humidity for the formulation containing more ionic liquid (left in figure 3.9), with the modulus decreasing as RH increases. A recent study [50] on the hygroscopicity of these compounds found that absorption of water could also be related to the anion in solution, with chloride being the prevalent one (which is the same mobile counterion in the polymeric samples produced for this work). Moreover, an increase of the modulus is experienced by samples obtained with the 10gly2peg formulation on the last week, a sign that maybe part of the water present in the IL solution tends to evaporate.
The formulation containing the most glycerol, on the other hand, seems to experience less variation.
In general, the sample were found to retain quite a lot of water as the weeks went by.

3.2.3 Electromechanical tests

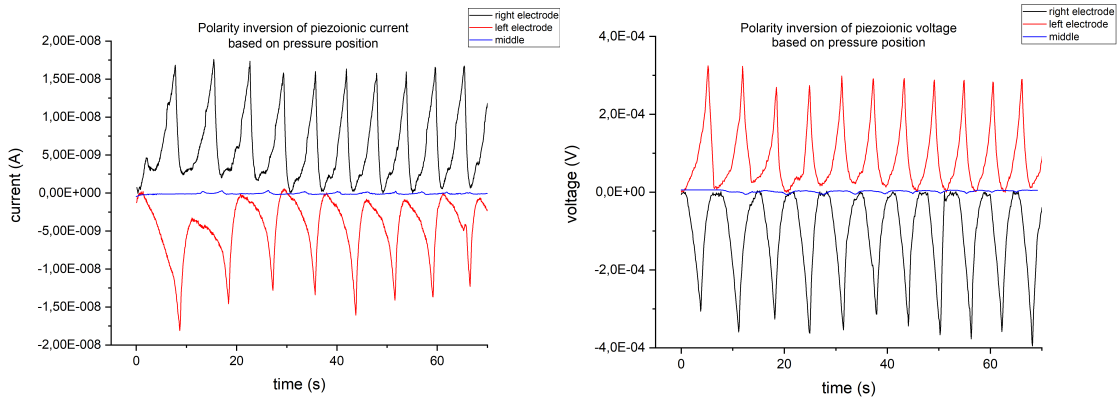

Figure 3.10: (left) current polarity inversion and (right) voltage polarity inversion as sample is pressed near electrodes and in the middle.

In figure 3.10 the polarity inversion of the piezoionic response can be appreciated. As the sample is pressed near the sense electrode (left electrode, in red in the figure), the Cl^- ions in the PIL solution are displaced towards the middle of the sensor. This creates an electric double layer (EDL) at the left electrode/matrix interface, with positive charges accumulating on it. As a result, electrons flow in the sense electrode and a negative current is detected.
The positive voltage tends to rise and then decays as the pressure is removed.
The opposite happens in the case of right electrode pressure, as the figure portrays. In the midde, the response detected is negligible. This is due to the fact that, under the indented region, a comparable amount of solvent flows in opposite directions towards the two electrodes, producing a concentration gradient of anions which is similar in magnitude but opposite in direction. As a result, a very small voltage (and thus current) is detected.
The phenomenon of polarity inversion based on touch location is one of the main aspects which make the piezoionic phenomenon interesting to investigate, as it paves the way for spatial recognition of touch in a way that's easy to implement.

In figure 3.11 and 3.12 the current and voltage response of dogbone samples prepared with the two formulations is reported.
The more rigid formulation presents a secondary peak, both in current and voltage, which is generated as the indenter detaches from the sample. The voltage decay seems also to be much slower.
On the right, the softer formulation presents a much faster decay. The successive peaks tend to start from a non-equilibrium position.

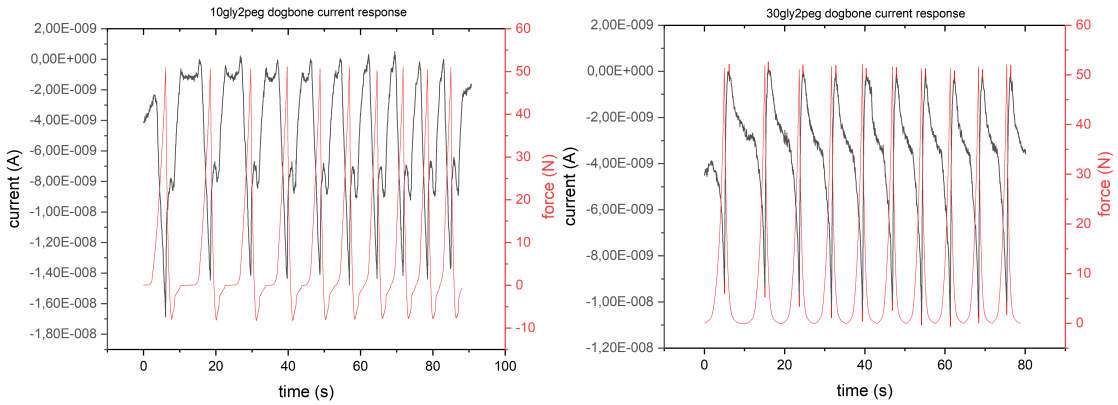

Figure 3.11: current waveform produced by (left) 10gly2peg and (right) 30gly2peg dogbone samples

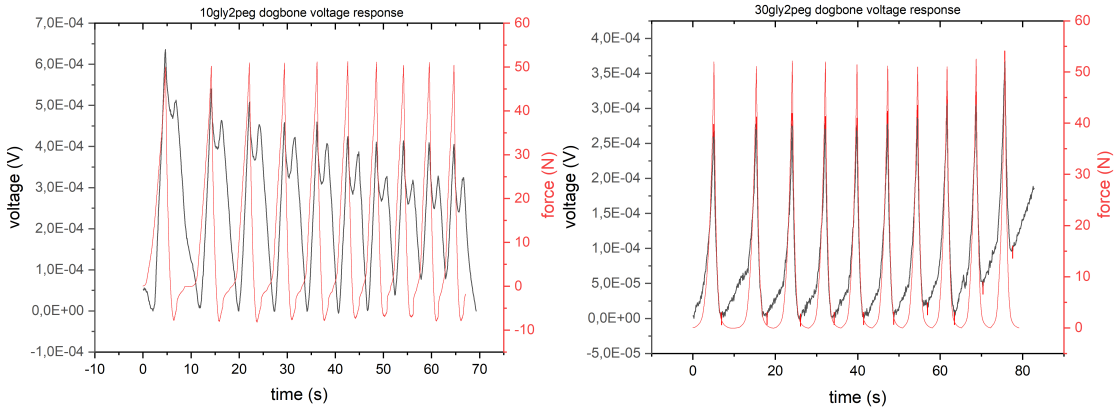

Figure 3.12: voltage waveform produced by (left) 10gly2peg and (right) 30gly2peg dogbone samples

This behavior can be attribute to stress relaxation of the polymer. The experiment is set up by applying a step force of 50N and monitoring the current decay (fig. 3.13, right). The resulting curve seems to experience an inital fast decay followed by a slower one.
The first part of the curve is fitted by an exponential function with a single time constant of the type

$$I = Aexp(-t/\tau) + I_0 \tag{3.1}$$

with I current, t time and τ characteristic time.
The τ extracted is 7,91s, which is comparable to the 6.62s between the first and second cycle in the right of fig 3.13. The appearance of a residual current can then be connected to the fact that as the force is removed, stress relaxation leads to

further ion separation, which persists until the next loading cycle begins. Additionally, a characteristic time of this length can be traced back to the choice of the matrix structure: it has in fact been reported [29] that in ionic liquid based iontronic touch sensors the charge separation tends to persist for longer times, in contrast to hydrogels swelled by acqueous salt solution, where the piezoionic response tends to drop rapidly.

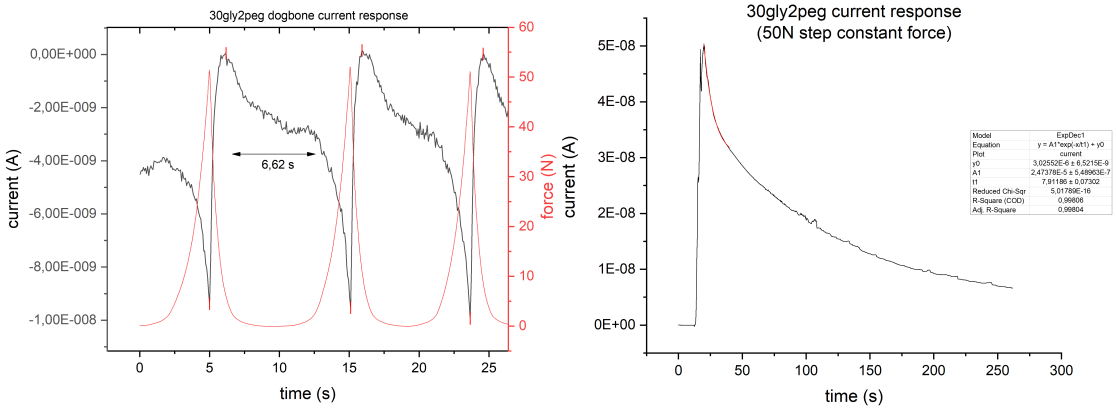

Figure 3.13: Current response to (left) cyclic loading and (right) to a single step compression

Another thing to note is that the longer relaxation time might also be due to the larger indenter size, which in this case had a square area of 10mm x 10mm. This phenomenon has been analyzed in [30] and the relevant figure is reported below, where longer voltage decay is observed as the indentation contact surface increases.

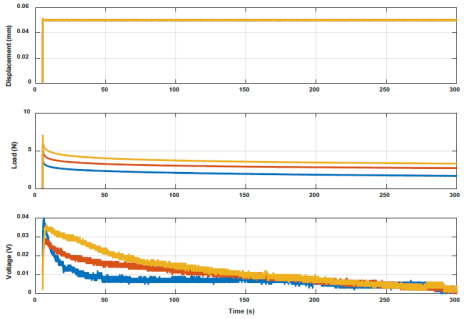

Figure 3.14: Load relaxation and voltage decay times corresponding to cilindrical indenter diameter of 10mm (yellow), 8mm (orange) and 6mm (blue), taken from [30] Supplementary Material

.

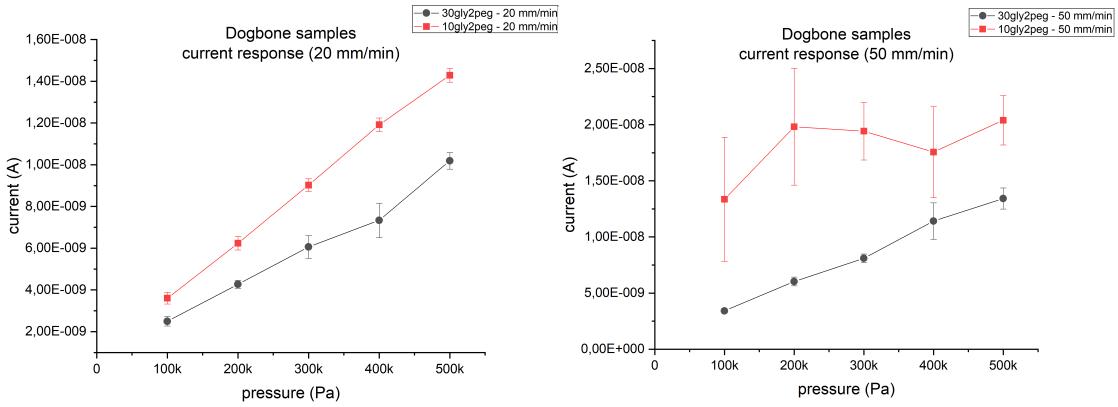

Figure 3.15: Current response to cyclic loading of the two type of dogbone sample for a crosshead speed of (left) 20 mm/min and (right) 50 mm/min

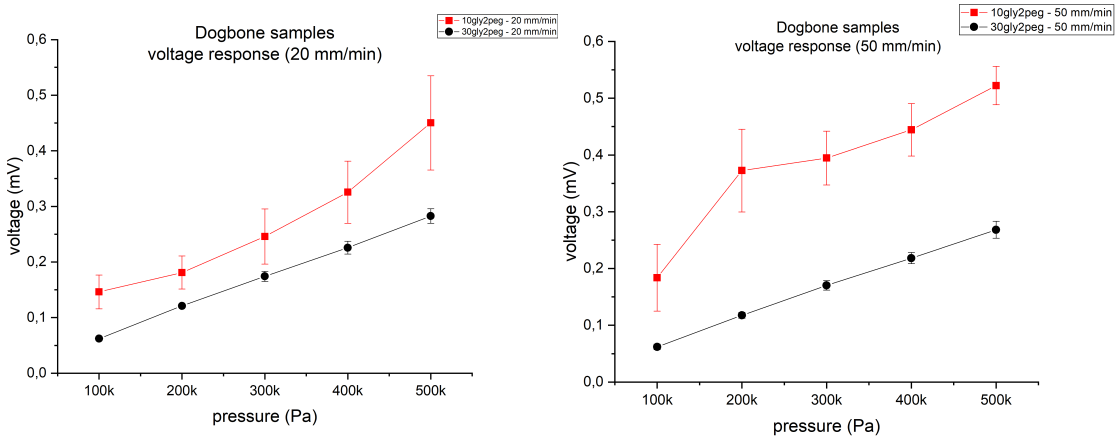

Figure 3.16: Voltage response to cyclic loading of the two type of dogbone sample for a crosshead speed of (left) 20 mm/min and (right) 50 mm/min

In figure 3.15 and figure 3.16 the current and voltage response of the dogbone samples at different pressures and for two testing velocities is reported. Each point in the graph is taken as the peak-to-peak amplitude averaged over 10 loading cycles. Sensors built using the formulation with the least amount of glycerol (10gly2peg) produce the highest signal in every case. This is due to the fact that these samples also contain more polymerized ionic liquid (88% v/v in the 10gly2peg case versus 68% v/v in the 30gly2peg case) and so more mobile counterions whose concentration gradient can be exploited for the production of a piezoionic voltage.
To be noted is the fact that the softer formulation seems to lead to a more linear response.

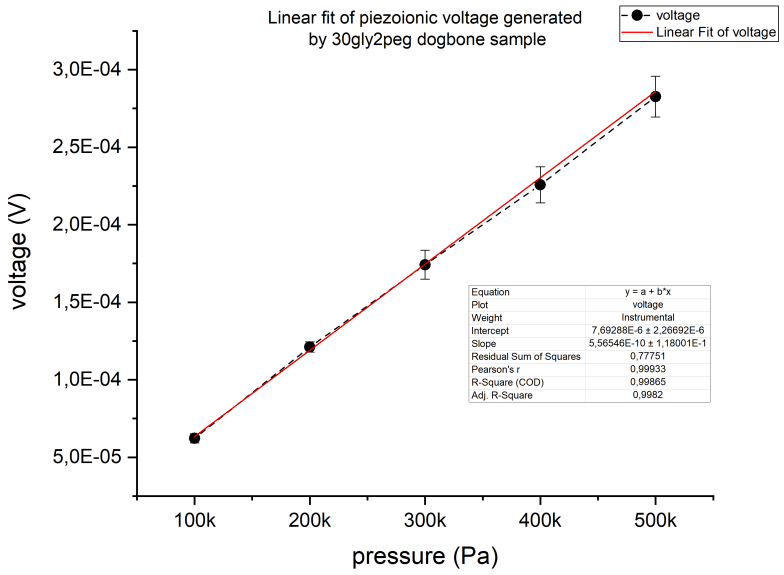

Figure 3.17: Linear fit of piezoionic voltage response for the 30gly2peg formulation

.

A linear fit of the voltage-pressure response for the less stiff samples leads to a piezoionic coefficient $\alpha = 0.0556 \times 10^{-10}$ nV/Pa. The parameter extracted is considered as the slope of the fit. This value is on the lower end of the range reported in [30] and more optimized materials may also reach 100 nV/Pa.

In figure 3.18 and figure 3.19 the electrical response of the square samples to ten loading-unloading force cycles is reported.
Although the current seems to behave quite linearly, especially in the softer formulation, the voltage seems to behave randomly.
The sandwich configuration for the square samples is in particular problematic and probably not suitable for measuring a piezoionic voltage. This is due to the fact that, as the pressure arrives from the top plate, ions tend to displace in a direction parallel to the plane where the sample lies (meaning they displace towards the left and the right). In this configuration the electrodes are placed on the top and the bottom, which means the potential difference detected might not directly correlate to the ions' displacement, at least in the case of samples with a reduced vertical thickness such as the ionic liquid square ones.

Finally, in figure 3.20 the strain experienced by the square sample as a function of pressure is compared to the current produced. The maximum deformation achieved

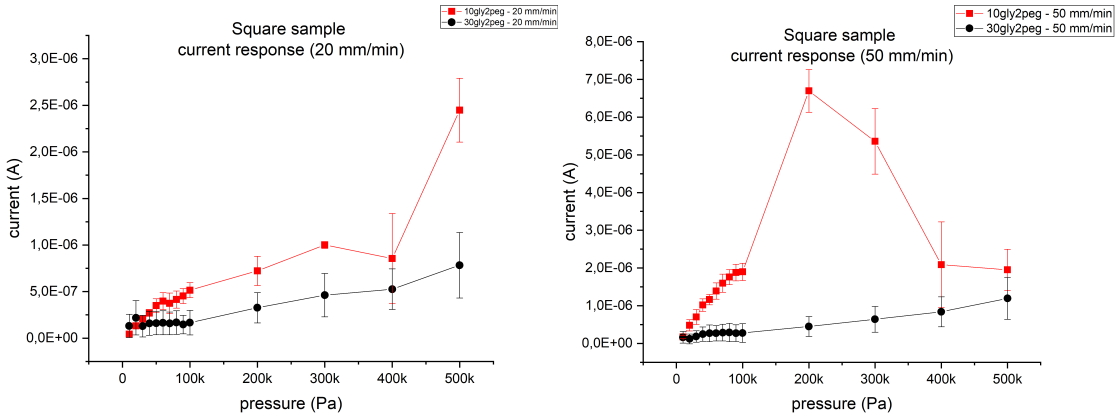

Figure 3.18: Current response to cyclic loading of the two type of square sample for a crosshead speed of (left) 20 mm/min and (right) 50 mm/min

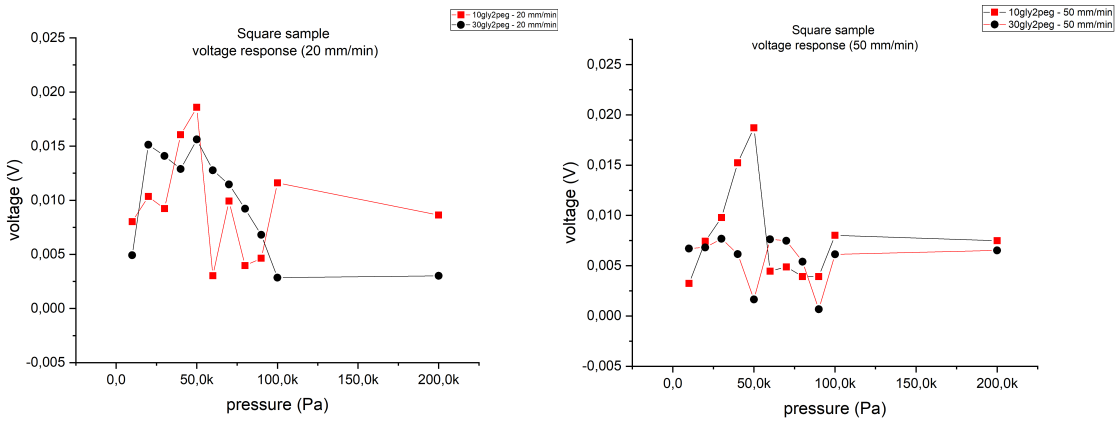

Figure 3.19: Voltage response to cyclic loading of the two type of square sample for a crosshead speed of (left) 20 mm/min and (right) 50 mm/min

by the polymer tends to saturate as the force increases, with the formulation possessing lower elastic modulus reaching higher strain values (at equivalent pressure). This indicates that at high stress the entire matrix might be flowing, changing the ion separation dynamic. Consequently, the current produced seems to reach saturation as well.
This behavior, also reported for the piezoionic voltage response [29], has not been demonstrated in this work, as static compression tests are probably necessary for it to be detected.

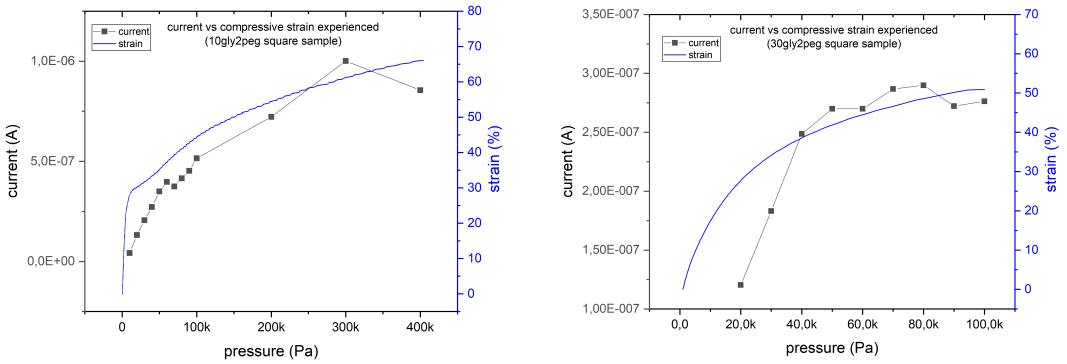

Figure 3.20: Current and strain relation to the applied stress on the square samples of (left) 10gly2peg formulation and (right) 30gly2peg fomulation

3.2.4 Physiological signal monitoring

Finally, dogbone sensors built with the formulation with the most amount of glycerol, 30gly2peg, were used to monitor physiological signals. The formulation chosen assured higher conformability of the sensor to the skin which should assure a better signal repeatability. The drawback is a lower signal produced, as demonstrated before.

In figure 3.21, the bending of a finger is recorded. To achieve this, the sensor was placed on the aforementioned location, with the sample's midpoint approximately on the interphalangeal joint. Polymide and duct tape were used to provide stability to the setup. The sensor's electrode were then connected to the Keithley 2400 multimeter.
As it can be seen from the current response, the sample is able to follow single events as well as multiple ones in succession. The flexion movement is associated to the rising edge of the signal and the extension to its decay. By keeping the finger bent, the current tends to drop slowly, as the diffusive back-current reduces the ions' separation to which current injection/extraction from the electrodes is followed.

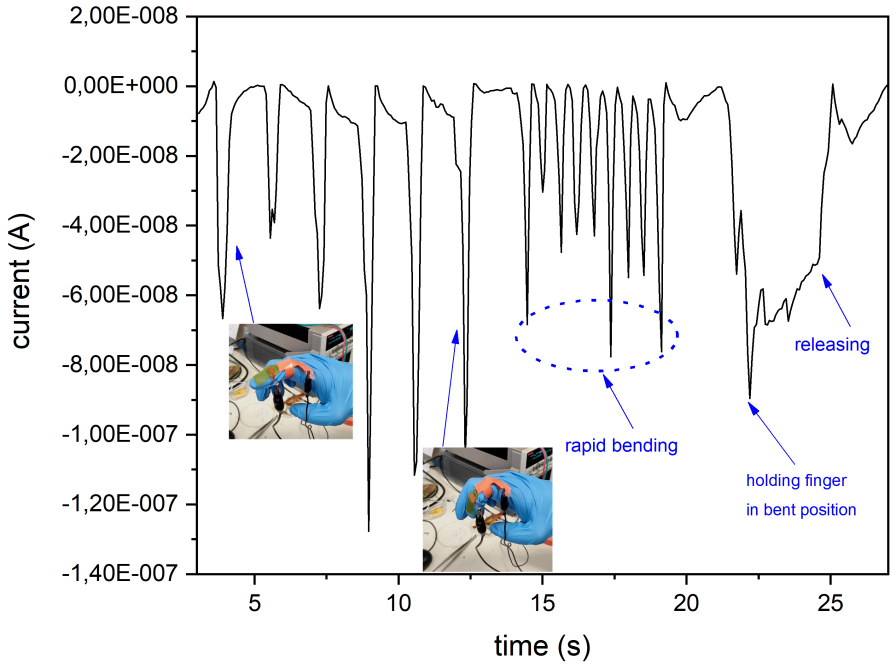

Figure 3.21: Current response to finger bending

.

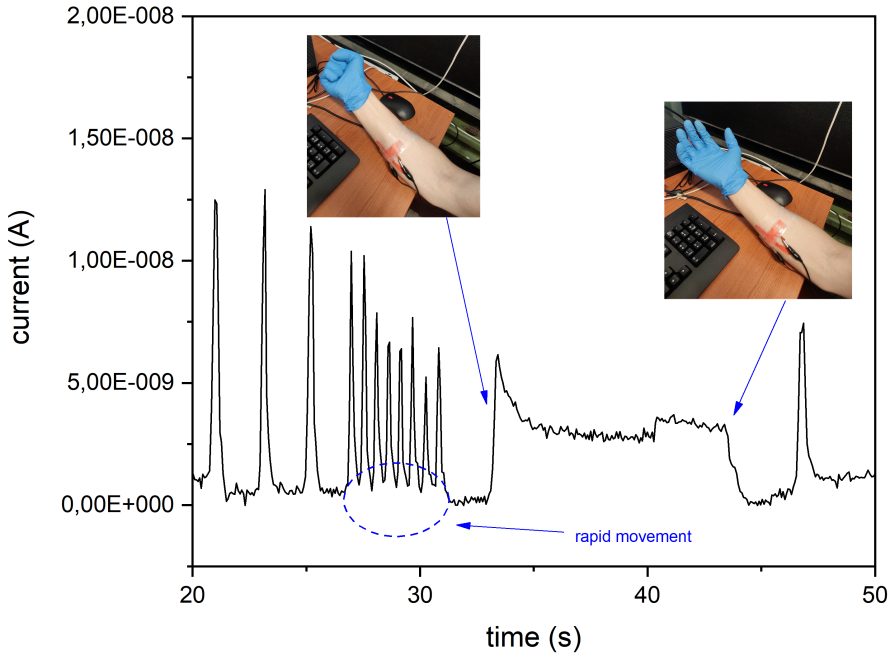

Figure 3.22: Current response to forearm flexor muscle engagement through palm closing

.

The response to the activation of the forearm flexor muscles through palm closing can be appreciated in figure 3.22. In this case the sensor is secured firmly to the forearm with Parafilm and connected to the electrical measurement tool as in the previous case. Both low and high frequency dynamic movements are performed and the sensor is able to follow through in this case as well.
Once again, a static motion in the form of holding the palm closed produces a slow signal decay, which becomes faster as the palm is opened.

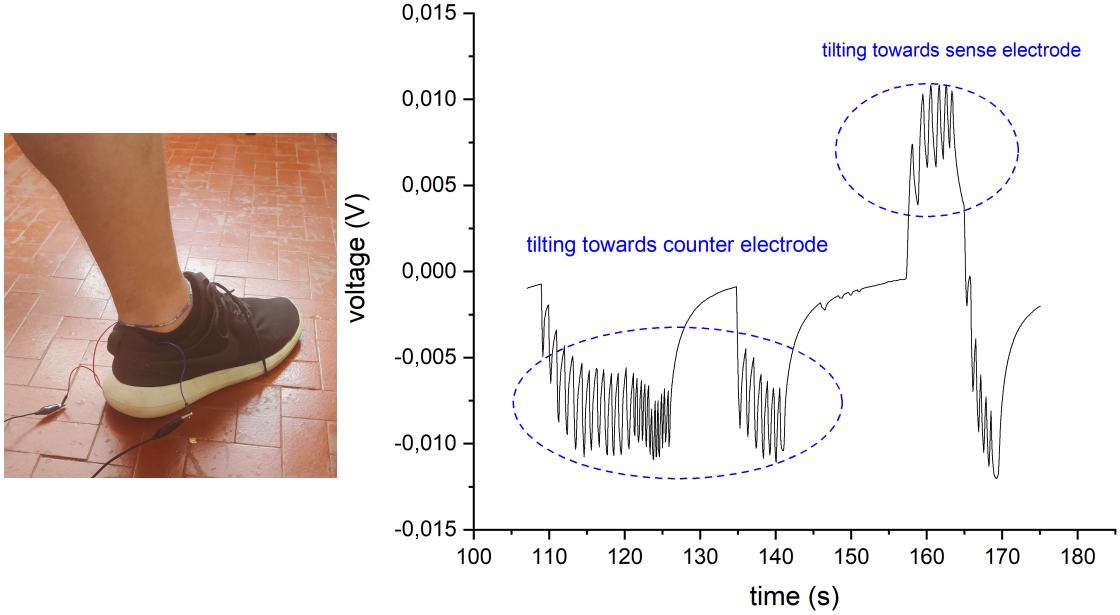

Figure 3.23: (left) positioning of the sensor in the insole and (right) voltage waveform obtained by tilting foot and pressing the shoe on the ground

As a last test, the sensor was mounted inside the insole of a patient (fig. 3.23, left) who was instructed to tilt his foot and exert pressure on the ground repeatedly. The scenario recreated may possibly pave the way for the application of these sensors in low-grade energy harvesting.
The voltage response, shown on the right of fig.3.23, confirms the inversion of polarity of the signal produced based on the orientation of tilting.

It has to be said that in all the tests performed the polymer is subjected to both compressive and tensile stress, reason for which the amplitude of the signal might differ from the usual recorded with the cyclic loading tests at the tensile machine. Nonetheless, these findings demonstrate the ability of piezoionic sensors to follow both static and dynamic motions with a sufficient degree of repeatability, all while being intrinsically self powered.

Chapter 4

Conclusion, limits and future studies

In this thesis work, the piezoionic effect as a novel means of mechanical-to-electrical transduction was investigated.
The initial electromechanical characterization of DLP 3d-printed cellulose samples allowed to gain insight on how the geometry might affect the stability of the response and the waveform produced. An high deformability of the sample was found to lead to enhanced voltage generation.
In order to investigate an alternative method for producing a piezoionic voltage, a formulation containing two notably green components, an ionic liquid (MAETAC) and glycerol was prepared. The addition of a crosslinker (PEGDA-700) and a photoinitiator (TPO-SDS) were necessary for the formation of a polymerized ionic liquid from the initial monomer.
The solution was poured in PDMS molds and then photocrosslinked using an UV lamp under N_2 exposure. Dogbone samples were characterized for their mechanical properties in tensile tests using an Instron Z5 tensile tester. Dogbone and square samples were characterized electromechanically coupling the tensile tester to a Keithley multimeter.
The increase in glycerol led to higher elasticity of the sample. Unfortunately, this component also decreased the electrical response produced. Nonetheless, linearity was achieved over a wide pressure range and the response saturation behavior typical of the piezoionic effect detected.

Future studies could focus on FEM simulation of different structures as a mean to optimize stress gradients produced while keeping an high compressibility of the sample. This should in theory increase the voltage generated for a given material

chosen, as the electric field generated by the ions' displacement is proportional to the pressure gradient.

Furthermore, tools like Comsol Multiphysics could be used to couple the structural mechanics simulation with the Darcy's law, Transport of Diluted Species and Electrostatics modules to develop a model of the piezoionic effect.
In this way the influence of material parameters (such as matrix porosity, solvent viscosity, type of ions in solution) and external ones (such as deformation/stress intensity and even indenter diameter) would be related to the electrical response. A good starting point is given in [51].

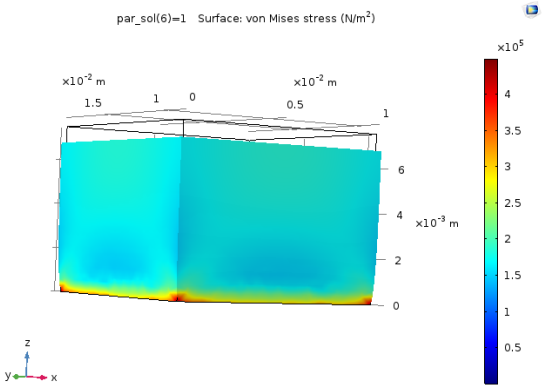

Figure 4.1: Comsol Multiphysics 6.1 stress simulation of cube geometry

.

Regarding the formulation, improvements need to be made on its stability and mechanical properties. The reduction of glycerol in solution might reduce the stickyness and hygroscopicity of the samples, characteristics which are detrimental for the measurement of the electrical response. Another approach could be to remove glycerol from the matrix altogether and soak the polymerized samples in a glycerol/water solution, as Odent et al did in [29].

Varying the amount of crosslinker (while keeping it under 10% v/v to avoid excessive sample rigidity) could also be interesting, as it has been reported [29] that an higher amount of this component is related to a decrease in ionic conductivity and thus in sense voltage (eq. 1.11).

3d printing of the resin could be achieved by introducing another component such as acrylamide (AAm) or acrylic acid (AA). Acrylic acid in particular, might not be optimal in high amount since at neutral pH it is deprotonated and might affect the response of the Cl^- counterions in solution. In general, a component capable of

increasing the elastic modulus (to facilitate the creation of self-standing structures) without a large increase of hysteresis losses in compression cycling should be preferred.
All of this has to be done while taking into account that reducing too much the amount of polymerized ionic liquid (and thus the concentration of moving ions available for conduction) can also reduce the amount of voltage produced.

Concluding, the field of piezoionics looks certainly promising for the implementation of an all-polymeric sensing platform.
These sensors' intrinsic self-powered abilities and capability to detect the location of an applied stimulus have been demonstrated here.
Furthermore, as it has been seen, their response can be tuned through material engineering and additive manifacturing tecniques, providing additional paths to explore towards an alternative method for human motion detection and beyond.

Bibliography

[1] Amira J. Zaylaa and Ahma El Hajj. «Neurocomputing and interfacing digital tasting system: research, design and evaluation». In: *BAU Journal* 4 (2023). DOI: 10.54729/2959-331X.1100.

[2] Catherine L. Reed. «Mechanoreceptors and Afferent Nerve Fibers». In: *Encyclopedia of the Human Brain* (2002).

[3] Anantha Ramana Vellipuram Franklin Iheanacho. *Physiology, Mechanoreceptors*. URL: https://www.ncbi.nlm.nih.gov/books/NBK541068.

[4] URL: https://humanphysiology.academy/Neurosciences%5C%202015/Chapter%5C%202/P.2.1%5C%20%5C%5CAfferents.html.

[5] M. Cutkosky W. Provancher. «On tactile sensing and display». In: *PhD Thesis* (2003).

[6] Z. Wang et al. W. Lin. «Self-Adaptive Perception of Object's Deformability with Multiple Deformation Attributes Utilizing Biomimetic Mechanoreceptors». In: *Adv. Mater.* (2024). DOI: 10.1002/adma.202305032.

[7] Kerun Liu, Weiwei Chen, Weimin Yang, Zhiwei Jiao, and Yuan Yu. «Review of the research progress in soft robots». en. In: *Appl. Sci. (Basel)* 13.1 (Dec. 2022), p. 120.

[8] Zhengya Shi, Lingxian Meng, Xinlei Shi, Hongpeng Li, Juzhong Zhang, Qingqing Sun, Xuying Liu, Jinzhou Chen, and Shuiren Liu. «Morphological engineering of sensing materials for flexible pressure sensors and artificial intelligence applications». en. In: *Nanomicro Lett.* 14.1 (July 2022), p. 141.

[9] C. Seesaard T.;Wongchoosuk. «Flexible and Stretchable Pressure Sensors: From Basic Principles to State-of-the-Art Applications». In: *Micromachines* (2023). DOI: 10.3390/mi14081638.

[10] Rui Xiao Cheng Zhang Xiaofan Gou. «Hysteresis in glass microsphere filled elastomers under cyclic loading». In: *Polymer Testing* (2021). DOI: 10.1016/j.polymertesting.2021.107081.

[11] Jiankun Huang, Jingbin Zeng, Xue Zhang, Gengchen Guo, Rui Liu, Zifeng Yan, and Yadong Yin. «Fatigue resistant aerogel/hydrogel nanostructured hybrid for highly sensitive and ultrabroad pressure sensing». In: *Small* 18.1 (Jan. 2022), e2104706.

[12] Yanjin Zhao, Ningfang Song, Fuyu Gao, Xiaobin Xu, and Zihang Gao. «Temperature-induced inconsistency in the pressure sensitivity of polymer-diaphragm-based FP pressure sensors». In: *Opt. Mater. Express* 13.3 (Mar. 2023), p. 687.

[13] Xin Yan Wufan Chen. «Progress in achieving high-performance piezoresistive and capacitive flexible pressure sensors: A review». In: *Journal of Materials Science Technology* (2020), pp. 175–188. DOI: 10.1016/j.jmst.2019.11.010.

[14] Songlin Su, Xuefeng Zhang, Dongrui Dang, Zhengdong Wang, and Zhixue Tong. «A high-performance flexible capacitive pressure sensor with 3-D printed hemispherical graded microstructures». In: *IEEE Sens. J.* 24.5 (Mar. 2024), pp. 5966–5975.

[15] Yan Zhong, Fucheng Gu, Longgang Wu, Jiaqi Wang, Shengping Dai, Hao Zhu, Guanggui Cheng, and Jianning Ding. «Porous conductive electrode for highly sensitive flexible capacitive pressure sensor over a wide range». en. In: *J. Alloys Compd.* 934.167919 (Feb. 2023), p. 167919.

[16] Kai Zheng, Fan Gu, Hongjin Wei, Lijie Zhang, Xi'an Chen, Huile Jin, Shuang Pan, Yihuang Chen, and Shun Wang. «Flexible, permeable, and recyclable liquid-metal-based transient circuit enables contact/noncontact sensing for wearable human-machine interaction». In: *Small Methods* 7.4 (Apr. 2023), e2201534.

[17] Andris Šutka et al. «Recycled polystyrene waste to triboelectric nanogenerators: Volumetric electromechanically responsive laminates from same-material contact electrification». In: *Adv. Energy Sustain. Res.* 5.6 (June 2024).

[18] Peter C Sherrell et al. «Probing contact electrification: A cohesively sticky problem». In: *ACS Appl. Mater. Interfaces* 13.37 (Sept. 2021), pp. 44935–44947.

[19] Aiswarya Baburaj, S K Naveen Kumar, Akshaya Kumar Aliyana, Megha Banakar, Satyaranjan Bairagi, and George Stylios. «Factors affecting the performance of flexible triboelectric nanogenerators (F-TENGs) and their sensing capabilities: A comprehensive review». In: *Nano Energy* 118.108983 (Dec. 2023), p. 108983.

[20] Kunming Shi, Bin Chai, Haiyang Zou, Zhen Wen, Yijie Liu, Meng He, Jie Chen, Pingkai Jiang, and Xingyi Huang. «Direct-current triboelectric nanogenerators based on contact–separation mode and conductive–adhesive interface». en. In: *Adv. Funct. Mater.* (Mar. 2024).

[21] Congju Li, Ran Cao, and Xiuling Zhang. «Breathable materials for triboelectric effect-based wearable electronics». en. In: *Appl. Sci. (Basel)* 8.12 (Dec. 2018), p. 2485.

[22] Wasim Akram, Qian Chen, Guangbo Xia, and Jian Fang. «A review of single electrode triboelectric nanogenerators». In: *Nano Energy* 106.108043 (Feb. 2023), p. 108043.

[23] Wenwu Zhu, Jun Peng, Ao Qin, Kang Long Yuan, Bo Shi Zhu, Shuai Lang, Ji Liang Ma, Guangrui Wen, and Xuefeng Chen. «Performance optimizations and figure-of-merits for freestanding triboelectric nanogenerators». 2024.

[24] Zhicai Yu, Zhenyu Zhu, Yingzi Zhang, Xiaoqian Li, Xin Liu, Yi Qin, Zhenrong Zheng, Lianyang Zhang, and Hualing He. «Biodegradable and flame-retardant cellulose-based wearable triboelectric nanogenerator for mechanical energy harvesting in firefighting clothing». en. In: *Carbohydr. Polym.* 334.122040 (June 2024), p. 122040.

[25] Nannan Wang, Yupeng Liu, Enyi Ye, Zibiao Li, and Daoai Wang. «Innovative technology for self-powered sensors: Triboelectric nanogenerators». en. In: *Advanced Sensor Research* 2.5 (May 2023), p. 2200058.

[26] Derek Ho. «The piezoionic effect: Biomimetic transduction mechanism for sensing, actuation, interface, and energy harvesting». en. In: *ChemElectroChem* 11.3 (Feb. 2024).

[27] Vincent Woehling, Giao T M Nguyen, Cedric Plesse, Yael Petel, Yuta Dobashi, John D W Madden, Carl A Michal, and Frederic Vidal. «Study of the piezoionic effect and influence of electrolyte in conducting polymer based soft strain sensors». In: *Multifunct. Mater.* 2.4 (Dec. 2019), p. 045002.

[28] Panadda Dechadilok and William M Deen. «Hindrance factors for diffusion and convection in pores». In: *Ind. Eng. Chem. Res.* 45.21 (Oct. 2006), pp. 6953–6959.

[29] Jérémy Odent, Nicolas Baleine, Valentin Biard, Yuta Dobashi, Cédric Vancaeyzeele, Giao T M Nguyen, John D W Madden, Cédric Plesse, and Jean-Marie Raquez. «3D-printed stacked ionic assemblies for iontronic touch sensors». en. In: *Adv. Funct. Mater.* 33.3 (Jan. 2023), p. 2210485.

[30] Yuta Dobashi et al. «Piezoionic mechanoreceptors: Force-induced current generation in hydrogels». en. In: *Science* 376.6592 (Apr. 2022), pp. 502–507.

[31] Young-Ryul Kim et al. «Bilayer piezoionic sensors for enhanced detection of dynamic, static, and directional forces with self-healing capabilities». en. In: *Nano Energy* 127.109749 (Aug. 2024), p. 109749.

[32] Chao Lu, Xi Chen, and Xiaohong Zhang. «Highly sensitive artificial skin perception enabled by a bio-inspired interface». en. In: *ACS Sens.* 8.4 (Apr. 2023), pp. 1624–1629.

[33] S Zohreh Homayounfar, Ali Kiaghadi, Deepak Ganesan, and Trisha L Andrew. «PressION: An all-fabric piezoionic pressure sensor for extracting physiological metrics in both static and dynamic contexts». In: *J. Electrochem. Soc.* 168.1 (Jan. 2021), p. 017515.

[34] Julian Smith-Jones, Nathan Ballinger, Naroa Sadaba, Xabier Lopez de Pariza, Yunxin Yao, Stephen L Craig, Haritz Sardon, and Alshakim Nelson. «3D printed modular piezoionic sensors using dynamic covalent bonds». en. In: *RSC Appl. Polym.* 2.3 (2024), pp. 434–443.

[35] Tom Grathwohl. *Microcrystalline cellulose and the pharmaceutical industry.* en. `https://www.pharmaexcipients.com/microcrystalline-cellulose-mcc-pharma/`. Accessed: 2024-7-5. Oct. 2020.

[36] Siti Nor Farhana Yusuf, Rosiyah Yahya, and Abdul Kariem Arof. «Ionic liquid enhancement of polymer electrolyte conductivity and their effects on the performance of electrochemical devices». In: *Progress and Developments in Ionic Liquids*. InTech, Feb. 2017.

[37] Salsabeel Al-Sodies, Abdullah M Asiri, Ajahar Khan, Khalid A Alamry, and Mahmoud A Hussein. «Recent exploiting of poly(ionic liquid)s in sensing applications». en. In: *Eur. Polym. J.* 205.112719 (Feb. 2024), p. 112719.

[38] Wangchuan Xiao, Quan Yang, and Shenlin Zhu. «Comparing ion transport in ionic liquids and polymerized ionic liquids». en. In: *Sci. Rep.* 10.1 (May 2020), p. 7825.

[39] Katarzyna Niesyto and Dorota Neugebauer. «Synthesis and characterization of ionic graft copolymers: Introduction and in vitro release of antibacterial drug by anion exchange». en. In: *Polymers (Basel)* 12.9 (Sept. 2020), p. 2159.

[40] Fabrício Mezzomo Collares, Vicente Castelo Branco Leitune, Patrícia Franken, Clarissa Fatturi Parollo, Fabrício Aulo Ogliari, and Susana Maria Werner Samuel. «Influence of addition of [2-(methacryloyloxy)ethyl]trimethylammonium chloride to an experimental adhesive». en. In: *Braz. Oral Res.* 31.0 (May 2017), e31.

[41] Christoph Hadler, Kirsten Wissel, Gudrun Brandes, Wibke Dempwolf, Günter Reuter, Thomas Lenarz, and Henning Menzel. «Photochemical coating of Kapton® with hydrophilic polymers for the improvement of neural implants». en. In: *Mater. Sci. Eng. C Mater. Biol. Appl.* 75 (June 2017), pp. 286–296.

[42] H J Chen, P Y Lee, C Y Chen, S L Huang, B W Huang, F J Dai, C F Chau, C S Chen, and Y S Lin. «Moisture retention of glycerin solutions with various concentrations: a comparative study». en. In: *Sci. Rep.* 12.1 (June 2022), p. 10232.

[43] Inayati, Damar Jati Pamungkas, and Maudy Pratiwi Novia Matovanni. «Effect of glycerol concentration on mechanical characteristics of biodegradable plastic from rice straw cellulose». In: *AIP Conference Proceedings*. Surakarta, Indonesia: Author(s), 2019.

[44] Robert Löwe, Thomas Hanemann, Tatiana Zinkevich, and Andreas Hofmann. «Structure-property relationship of polymerized ionic liquids for solid-state electrolyte membranes». en. In: *Polymers (Basel)* 13.5 (Mar. 2021), p. 792.

[45] *2-(Methacryloyloxy)ethyl trimethylammonium chloride H2O 75wt. 5039-78-1*. en. `https://www.sigmaaldrich.com/IT/it/product/aldrich/408107`. Accessed: 2024-7-4.

[46] *Poly(ethylene glycol) diacrylate*. en. `https://www.sigmaaldrich.com/IT/it/product/aldrich/455008`. Accessed: 2024-7-4.

[47] *Glycerol*. en. `https://www.sigmaaldrich.com/IT/it/product/sigma/g2025`. Accessed: 2024-7-4.

[48] A Y Lau and N M Sarbon. «Effect of glycerol concentrations on the mechanical and physical properties of chicken skin gelatin-tapioca starch composite films». en. In: *Food Res.* 6.4 (Aug. 2022), pp. 428–436.

[49] Takuma Matsuoka, Kikuna Kumagai, and Hiroshi Nonaka. «Thermal extrusion of cellulose using hydroxypropyl methylcellulose». en. In: *Cellulose* 29.5 (Mar. 2022), pp. 2975–2983.

[50] Esther Rilo, Alejandro Rosende-Pereiro, Montserrat Domínguez-Pérez, Oscar Cabeza, and Luisa Segade. «New insights into the hygroscopic character of ionic liquids: Study of fourteen representatives of five cation and four anion families». en. In: *Int. J. Mol. Sci.* 25.8 (Apr. 2024).

[51] Yuta Dobashi. *Characterization of ionic polymers : towards applications as soft sensors in medicine*. 2017.